

Constraining the Beam Neutrino MC Flux Using the MINOS ND Data

Sacha Kopp,² Žarko Pavlović,² Patricia Vahle¹, Rustem Ospanov²

¹University College, London, ²University of Texas at Austin

Abstract

This document describes a method to handle correlated systematic uncertainties from hadron production on the beam spectrum by using the neutrino data from the MINOS detector. We have developed a tuning function which can be applied after the fact to the Monte Carlo to force agreement with the CC neutrino energy spectra observed in the near detector and the beam MC. The method relies on the flexible NuMI beam, which can be configured so as to selectively sample pions of different momenta and angles off the target. There is sufficient information in the neutrino data in a detector like MINOS to deduce the portion of the underlying spectrum of hadrons off the NuMI target which contribute to the NuMI flux.

1 Introduction

The simulation of the beam flux consists of three portions: (1) the simulation of the creation of mesons via $p + C \rightarrow \pi^\pm X, K^\pm X$, (2) the tracking, scattering, and possible downstream interactions of these mesons through the horns, decay pipe, and shielding, and (3) the calculation of the weights of the resulting mesons to decay into a neutrino of a given energy which strikes the near or far detector. The flexible beam NuMI beam design [13], in which the target can be adjusted from LE→HE beams, and in addition the horn current can be changed, allows a powerful constraint or deconvolution of the systematic uncertainties from these key portions of the beam flux prediction.

The systematic uncertainties arising from (2) and (3) are documented in `minos-doc-1283`. These uncertainties include effects such as our knowledge of the absolute current flowing through the horns, the alignment of the horns and target to the rest of the beam line, the shielding geometry, *etc.* In `minos-doc-1283` we also gave correlated errors from these various effects on the neutrino spectra of the LE, ME, and HE beams. That is, if an error such as a misalignment of a horn has occurred, such error will cause a known percentage decrease in the flux at one neutrino energy, but may cause an increase in the flux at a higher neutrino energy.

It is clear that *ab initio* calculations of the neutrino flux from the NuMI beam are in error by inspection of Figure 1, In order for the flux calculation to agree with MINOS data, a downward shift of the beam MC by "one-sigma" at $E_\nu=10$ GeV in the LE beam is to be

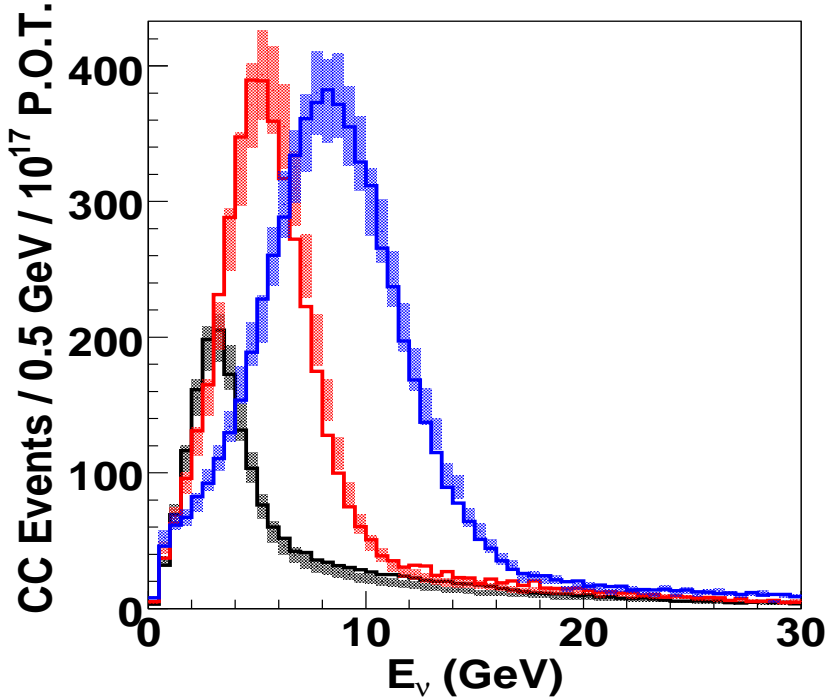


Figure 1: Comparison of the ND CC ν_μ sample selected by preselection cuts (no PID) with the GNuMI-v.18 beam MC. The error bands are dominated by hadron production estimated from two models for meson production in the target: MARS-v.15[17] and FLUKA2005[23].

accompanied by a downward or upward shift at this same energy in the ME or HE beams. While discrepancies between data and flux MC may be readily explained by virtue of detector effects, the fact that these discrepancies vary by beam setting indicate that knowledge of particle production off the target is the culprit.

Several previous experiments have used their neutrino data to constrain the yield of hadrons off the target, reducing uncertainties in the flux prediction [4, 5, 6, 7, 8]. The NuMI beam, with its flexible neutrino energy [9], provides an enhanced capability to constrain particle production. The capability of the NuMI beam to vary both the target position and the horns' current permits us to effectively map out particle production in (x_F, p_T) . Variation of I_{horn} focuses different $\langle p_T \rangle$ of hadrons. Variation of the target z location selects different hadrons' longitudinal momentum $\langle p_z \rangle = \langle p_T \rangle / \tan \theta = \langle p_T \rangle \frac{z_{target}}{r_{horn}}$. In the case of these past experiments, they could utilize a well-known scattering process (quasi-elastics for example) as the normalization mode to obtain a flux. In the present analysis with MINOS data, inclusive events are utilized, so an absolute flux cannot be obtained. The hope here is to show the feasibility of the method, so that it may be repeated using a well-known normalization mode in MINERvA.

As is demonstrated in Figure 2, pions account for the majority of the low ($E_\nu < 30$ GeV)

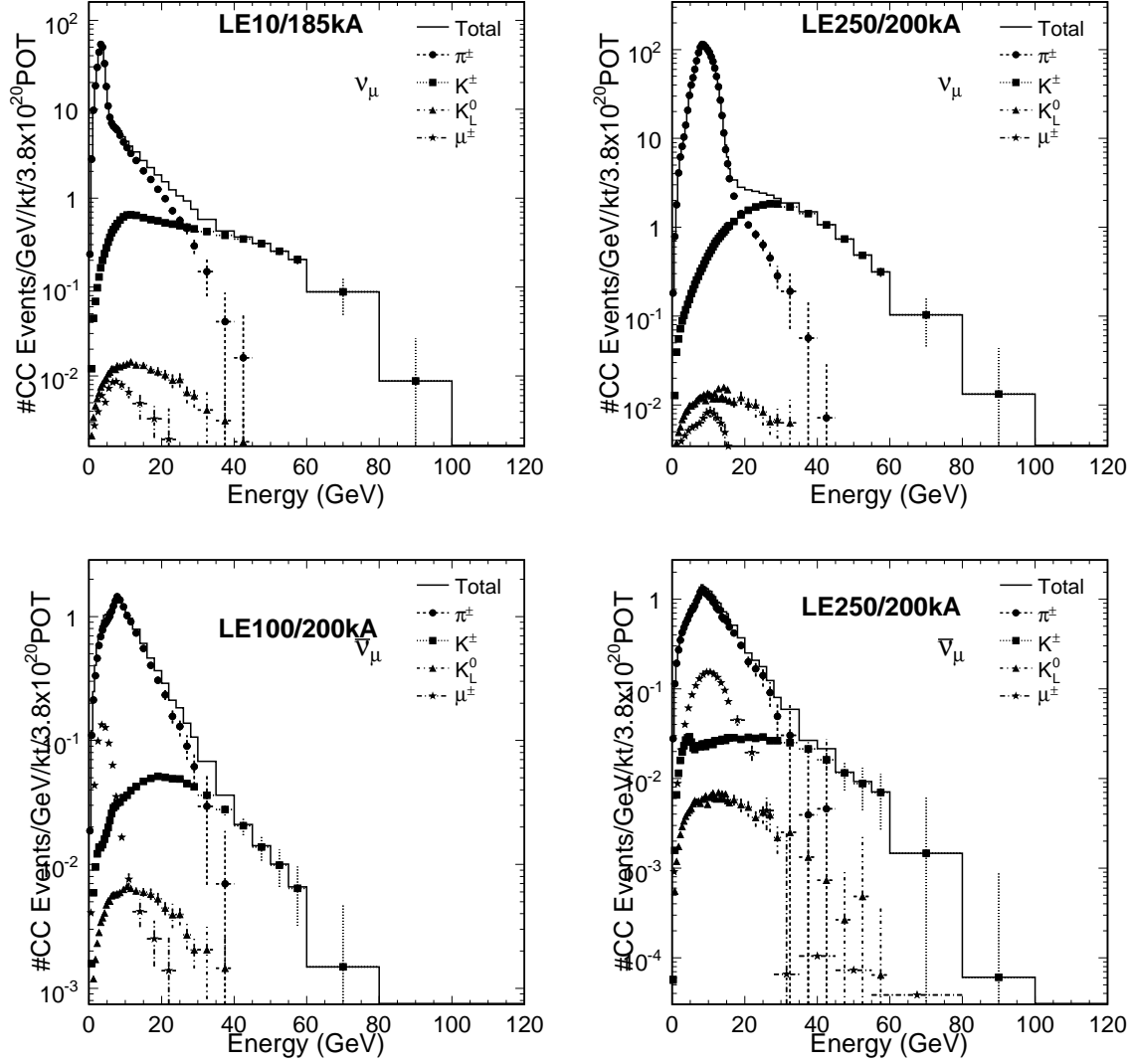


Figure 2: Charged current energy spectrum for ν_μ (top row) and $\bar{\nu}_\mu$ (bottom) in the Near Detector for two different configurations of the NuMI beam, along with contributions from each type of parent particle. The two configurations differ in the location of the target relative to the first horn and in the current in the horns.

neutrino flux, while charged kaons dominate at the high energies. Neutrinos from muon decays are less significant, and in any case are coupled to the rates from pion and kaon parents. Thus, by fitting the lower energy portion of the neutrino spectrum, we can learn something about the pion yield off the NuMI target, while high energy neutrinos teach us about the kaon yields. While the ν_μ flux from K_L^0 decays is quite small, the K_L^0 's contribute significantly to the ν_e flux. Later in this note, we discuss a scheme for approximating the K_L^0 flux from the K^\pm fluxes.

The goal of this paper is, by fitting the beam MC to the ND data, achieve the best flux and uncertainty for the NuMI beam. We show that the neutrino data in the MINOS ND data essentially acts as an additional hadron production data set. Further, the constraints on the ν_μ and $\bar{\nu}_\mu$ fluxes provide constraints on the ν_e and $\bar{\nu}_e$ fluxes.

2 Fitting for Hadron Production

Our default hadron production model in GNUMI-v.18 is the FLUKA2005 model[23], whose π^+ yield is shown in Figure 3.¹

The NuMI beam has been operated in 6 beam configurations which probe different regions of the production spectra in $x_F \approx p_z/p_{\text{proton}}$ and p_T space. By comparing the level of agreement of the ND data with the beam MC in these 6 configurations, it is possible to disentangle the source of various systematic discrepancies. The 6 beam configurations are:

- LE10: target at -10 cm from full insertion into the horn, horn pulsing at 185 kA.
- "horn off": target at -10 cm, horn at 0 kA
- "low horn": target at -10 cm, horn at 170 kA
- "high horn": target at -10 cm, horn at 200 kA
- pME: target at -100 cm, horn at 200 kA (LE100/200kA)
- pHE target at -250 cm, horn at 200 kA (LE250/200kA).

For the first analysis based on 10^{20} POT, all but the horn off data has been used in the combined analysis to tune the beam spectrum. In the next round of analysis all 6 beams are used to tune the beam. Here are presented results of the fits to 6 beams. Results of the fit to 5 beams can be found in appendix.

Figure 4 shows the distribution of $x_F \approx p_z^\pi/p_{\text{proton}}$ and p_T of pions at their creation in the target for those π^+ that give CC neutrino interactions in the ND. This figure is derived from Figure 3, but an additional weighting probability is applied for the pion to track through the horns, decay in the decay pipe, and the resulting muon neutrino to undergo a

¹It is interesting to note that the neutrino spectrum predicted with Fluka particles changed substantially between the Fluka-2001 and Fluka-2005 versions, despite the fact that no new data in our energy regime has become available in this time. The change was as much as 30% in the high energy tail of the LE beam.

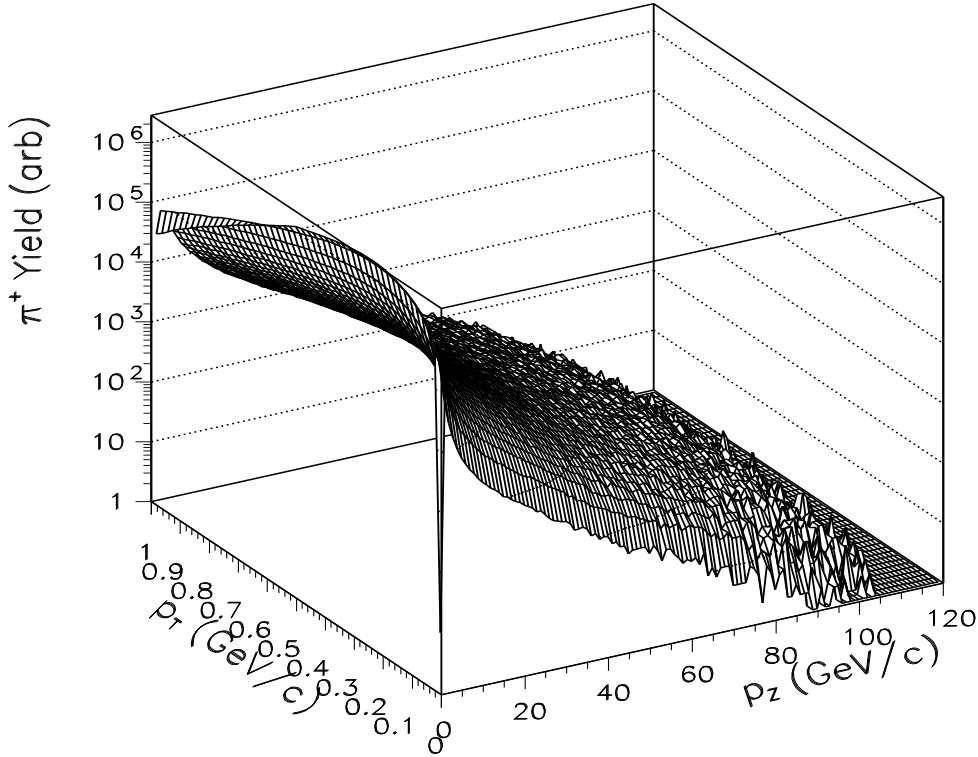


Figure 3: Yield of π^+ from the NuMI target as determined from a stand-alone FLUKA2005 simulation of the target geometry. Similar yields for π^- , K^\pm , etc, are derived. The yield is plotted as a function of p_z , the longitudinal momentum of the pion along the beam axis, and p_T , its momentum transverse to the beam axis.

CC interaction in the ND. Similar distributions are available from the beam MC for K^+ . We see that different beams sample different pions and this suggests that it should be possible to somewhat independently tweak each beam by changing the yields of pions of certain p_T and p_z .

For particles which are well-focused by the horns, there is a nearly linear relation between the pion p_z and its daughter E_ν , while for poorly-focused particles, this correlation is smeared. The relation

$$E_\nu = \frac{0.43E_\pi}{1 + (\gamma\theta)^2}$$

Thus, for a well-focused pion traveling parallel to the beam axis, the average pion decay angle to the ND is $\theta \sim 0$ and $E_\nu \approx 0.43E_\pi \approx 0.43p_z$. For a poorly-focused pion entering the decay pipe at an angle, the decay angle θ to hit the ND is on average non-zero and the resulting neutrino energy reduced.

This trend is seen in Figure 5, which shows the resulting neutrino energy spectra from

Model	$\langle p_T \rangle$ (GeV/c)
Fluka 2001[23]	0.43
Fluka 2005[23]	0.36
MARS-v.15[17]	0.38
Malensek[22]	0.50
Geant/Fluka[19]	0.37
Sanford-Wang[20]	0.42
CKP[21]	0.44

Table 1: Comparison of mean transverse momenta of π^+ from a thick graphite target struck by 120 GeV protons, as calculated by several interaction Monte Carlos.

two particular bins in the (x_F, p_T) plane: In the left plot of Figure 5, the neutrino spectra in the LE, ME, and HE beams are shown for pions which have $4 < p_z < 8$ GeV/c and $150 < p_T < 200$ MeV/c. Referring to Figure 4, one may note that this (x_F, p_T) bin is within the focusing peak of the LE and ME beams, but not the HE beam, thus it is not surprising that the HE component in Figure 5 is off-momentum. Likewise, the right plot of Figure 5 shows the neutrino spectra in the LE, ME, and HE beams for pions which have $16 < p_z < 20$ GeV/c and $150 < p_T < 200$ MeV/c

The relation between neutrino energy and (x_F, p_T) for the 6 beam configurations may therefore be used to weight up or down the pion flux in each (x_F, p_T) bin and thereby recalculate the resulting neutrino energy spectrum.

The yield of secondary hadrons from the target, and in particular the differential yield $d^2N/dp_T dx_F$, where p_T is the secondary's momentum transverse to the beam axis and $x_F \approx p_z/p_{proton}$ is the Feynman scaling variable (p_z is the secondary's momentum along the beam axis), is the dominant uncertainty in predicting the neutrino flux from the NuMI beam. Other uncertainties due to focusing errors or changing beam conditions were studied in [2] and are found to be small or manageable. Given the paucity of data from experiments of ≈ 120 GeV protons on Carbon targets, and the absence of data from thick targets, theoretical and empirical models [23, 17, 18, 22, 19, 21] which extrapolate or fit such data are poorly constrained and yield neutrino fluxes differ by 20-30%, as is discussed in Appendix A. Table 1, for example, lists predictions of a mean transverse momentum of positive pions from the target as predicted by different hadron production models.

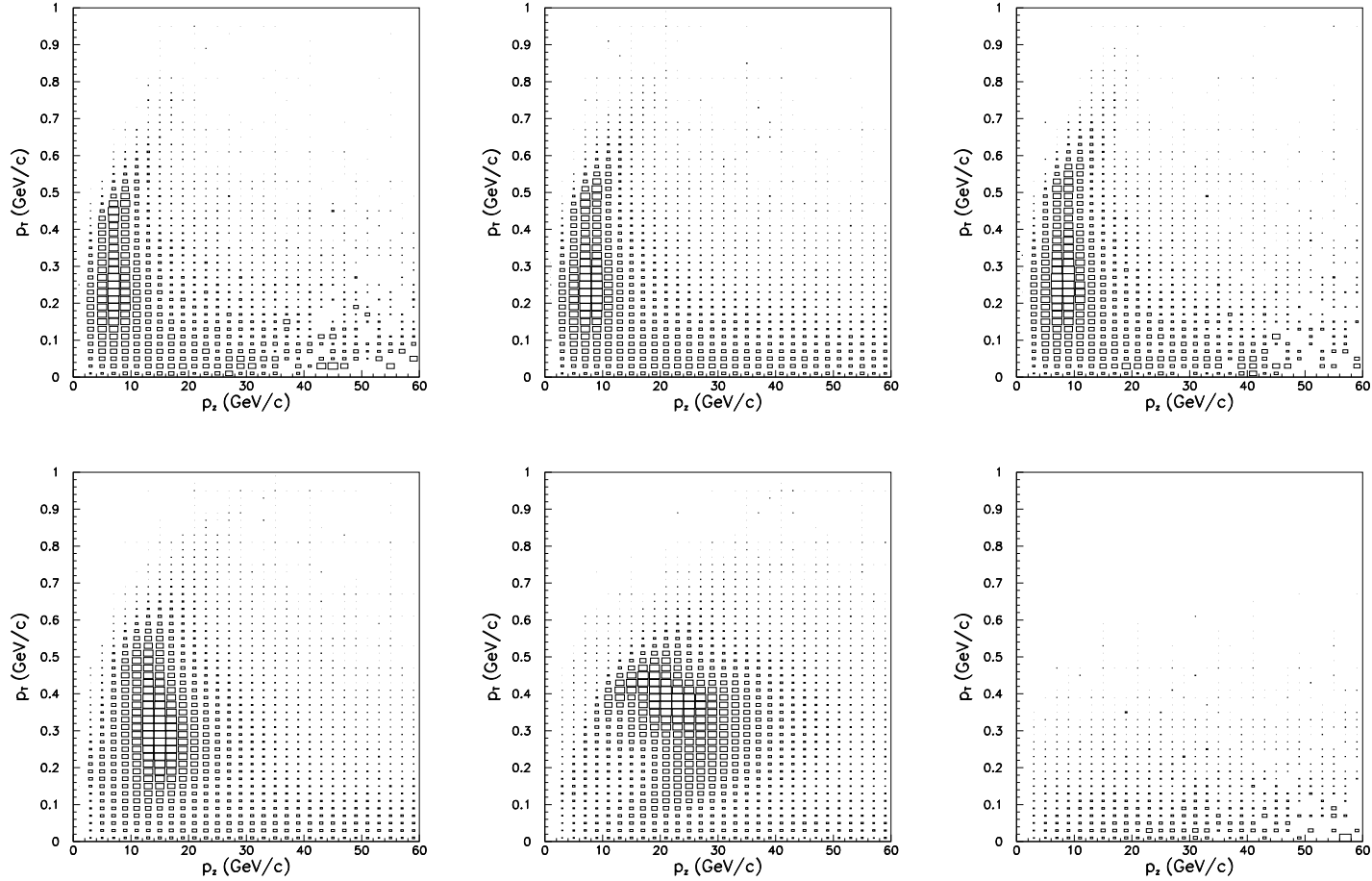


Figure 4: Distribution of p_T and x_F of π^+ that contribute to the the ND CC event rate. The box sizes are proportional to the probability of the pion resulting in a CC interaction in the ND. The 6 plots correspond to the 6 beam configurations which have been run: LE10/170kA (top left), LE10/185kA (top middle), LE10/200kA (top right), LE100/200kA (bottom left), LE250/200kA (bottom middle), horn off (bottom right). As is evident, each beam configuration samples different region of (x_F, p_T) .

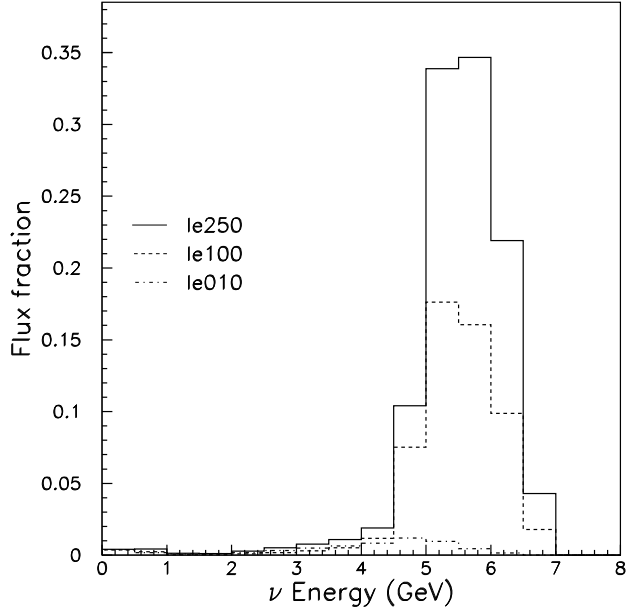
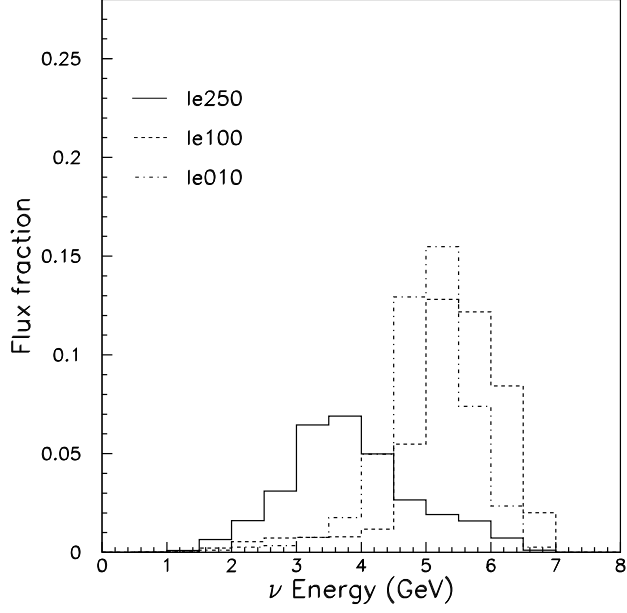


Figure 5: Contribution to E_ν spectrum from two different regions in the (p_z, p_T) plane: left: $4 < p_z < 8$ GeV/ c and $150 < p_T < 200$ MeV/ c . right: $16 < p_z < 20$ GeV/ c and $150 < p_T < 200$ MeV/ c . For each (p_z, p_T) bin, the neutrino spectra contributions to the LE, ME, and HE beams are shown.

3 Parameterized Tuning of Hadron Production

We fit the p_T-p_z distributions in Figure 3 of secondaries coming of the target as simulated by Fluka 2005[23]. The following functional form is used to fit the p_T distributions in different p_z (or equivalently x_F) bins:

$$\frac{d^2N}{dx_F dp_T} = [A + Bp_T] * \exp(-Cp_T^{3/2}) \quad (1)$$

A, B and C are the parameters in the fit. Fitting p_T distributions in different p_z bins gives us those three parameters as function of x_F . This functional form loosely follows the BMPT[18] parameterization. Parameter A determines the low p_T yields, B determines how fast the distribution rises and C determines the fall off at high p_T . With these parameters we can change the position of the peak of the distribution, its width and the total area under the curve (which is proportional to the total number of particles in that x_F bin). These are the knobs that we will need to make the fit to the ND data. Figures 6 and 7 show the p_T distributions of positive and negative pions and kaons from the NuMI target as given by Fluka2005, for several bins of x_F . Also shown as black curves in Figures 6 and 7 are the fits to the p_T distributions using Equation 1.

The parameters A , B , and C from these fits are themselves fit to the following functions $A(x_F)$, $B(x_F)$ and $C(x_F)$ to give parametric expressions as a function of x_F :

$$\begin{aligned} A(x_F) &= a_1 * (1 - x_F)^{a_2} * (1 + a_3 * x_F) * x_F^{-a_4} \\ B(x_F) &= b_1 * (1 - x_F)^{b_2} * (1 + b_3 * x_F) * x_F^{-b_4} \\ C(x_F) &= c_1/x_F^{c_2} + c_3 \quad (\text{for } x_F < 0.22) \\ &= c_1 e^{c_2(x_F - c_3)} + (c_4 x_F) + c_5 \quad (\text{for } x_F > 0.22) \end{aligned} \quad (2)$$

The fitted values of A , B , and C , together with the fitted functions from Equation 2, are shown for the π^+ yields in Figure 8. The coefficients a_i , b_i , and c_i for the functions $A(x_F)$, $B(x_F)$ and $C(x_F)$ are given in Table 2, and the parametric function for $d^2N/dx_F dp_T$ using Equations 1 and 2 are shown as the red curves in Figures 6 and 7. If the parameterization were perfect, the black and red curves would coincide, and the small discrepancies arise from the imperfect parameterizations in Equations 2. Nonetheless, this parameterization shows satisfactory agreement with Fluka 2005 predictions. As it will become obvious in the Section 4, it is not necessary to get the perfect agreement here since the aim of this procedure is just to get the knobs that can be used to tweak the hadron production.

Coefficient		a_i	b_i	c_i	
				$(x_F < 0.22)$	$(x_F > 0.22)$
π^+	1	-0.7607E-02	0.5465E-01	-0.7058E+01	0.3008E+01
	2	0.4045E+01	0.2675E+01	0.1419E+00	-0.1984E+00
	3	0.9620E+04	0.6959E+05	0.9188E+01	0.3577E+01
	4	0.2975E+01	0.3144E+01		0.2616E+01
	5				0.1225E+00
K^+	1	-0.5187E-02	0.4918E+00	-0.1610E+02	0.6905E+01
	2	0.4119E+01	0.2672E+01	-0.4582E-01	0.1630E+00
	3	0.2170E+04	0.1373E+04	0.1792E+02	0.6718E+01
	4	0.2767E+01	0.2927E+01		-0.4257E+00
	5				0.2486E+01
π^-	1	-0.6306E-02	0.4608E-01	-0.1652E+02	0.2972E+01
	2	0.5730E+01	0.3291E+01	-0.6204E-01	-0.1758E+00
	3	0.1365E+05	0.5857E+05	0.1812E+02	0.2266E+01
	4	0.2900E+01	0.3209E+01		0.1730E+01
	5				0.4196E-01
K^-	1	-0.8854E+01	0.2857E-01	-0.1613E+02	0.3916E+01
	2	0.6778E+01	0.7494E+01	-0.5678E-01	0.4615E+01
	3	-0.6050E+00	0.5879E+05	0.1739E+02	0.3255E-01
	4	0.1827E+01	0.2577E+01		-0.4702E+01
	5				0.4062E+00

Table 2: Coefficients of the fits of Figures 6 and 7 to Equations 1 and 2.

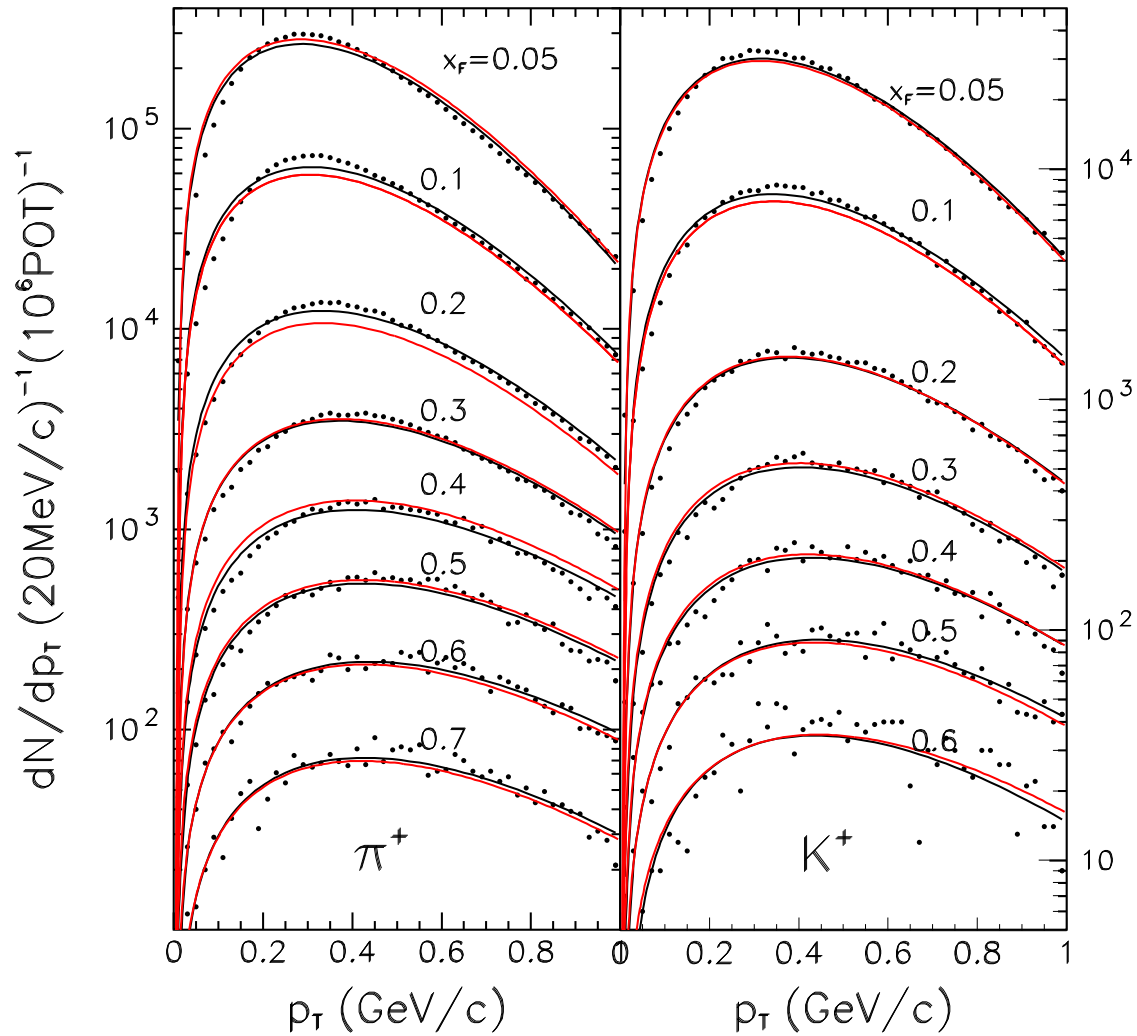


Figure 6: Fit to Fluka 2005 yields of π^+ and K^+ . The black dots are Fluka 2005, black solid line is the fit to each particular x_F slice using Equation 1 and red line is the overall fit using Equation 2.

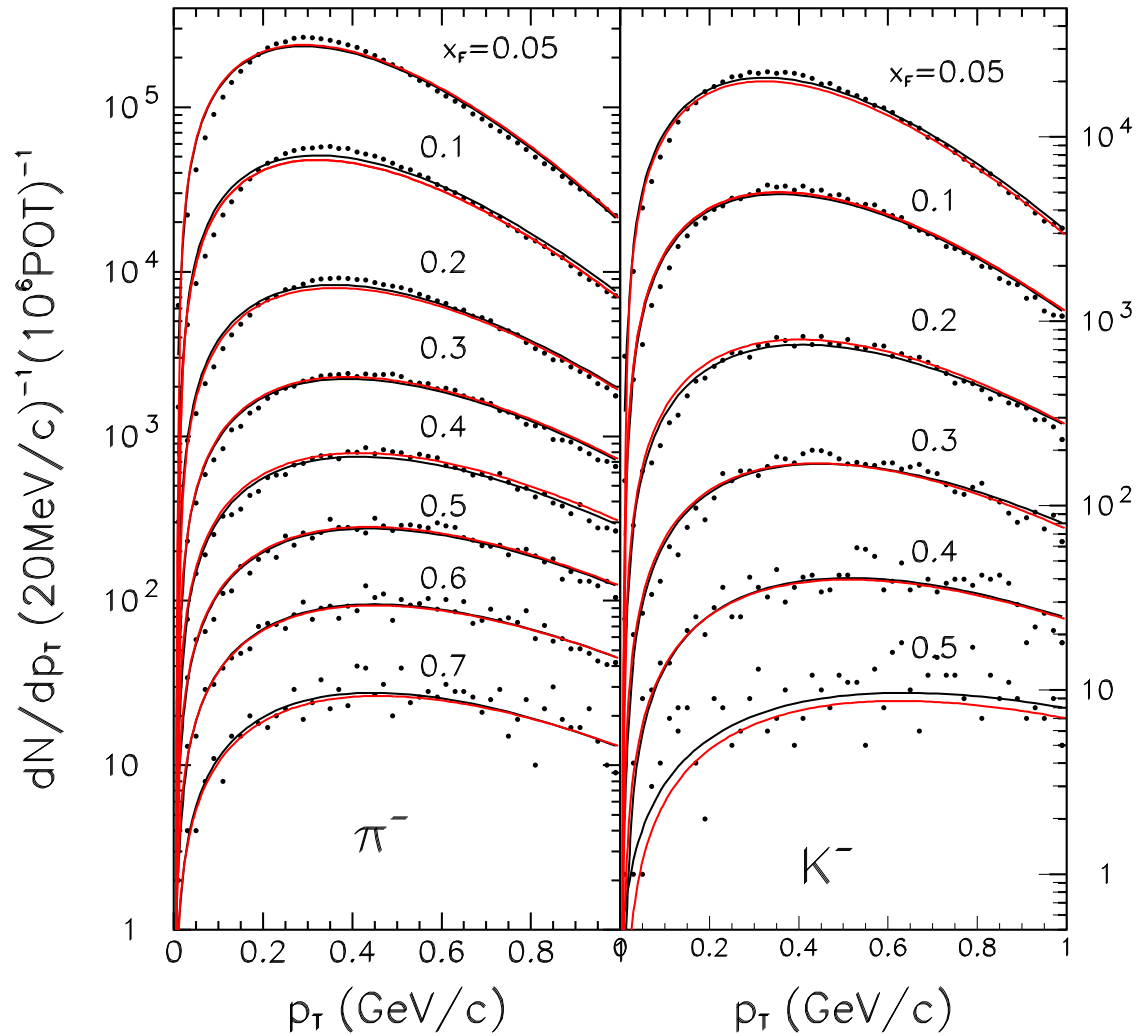


Figure 7: Fit to Fluka 2005 yields of π^- and K^- . The black dots are Fluka 2005, black solid line is the fit to each particular x_F slice using Equation 1 and red line is the overall fit using Equation 2.

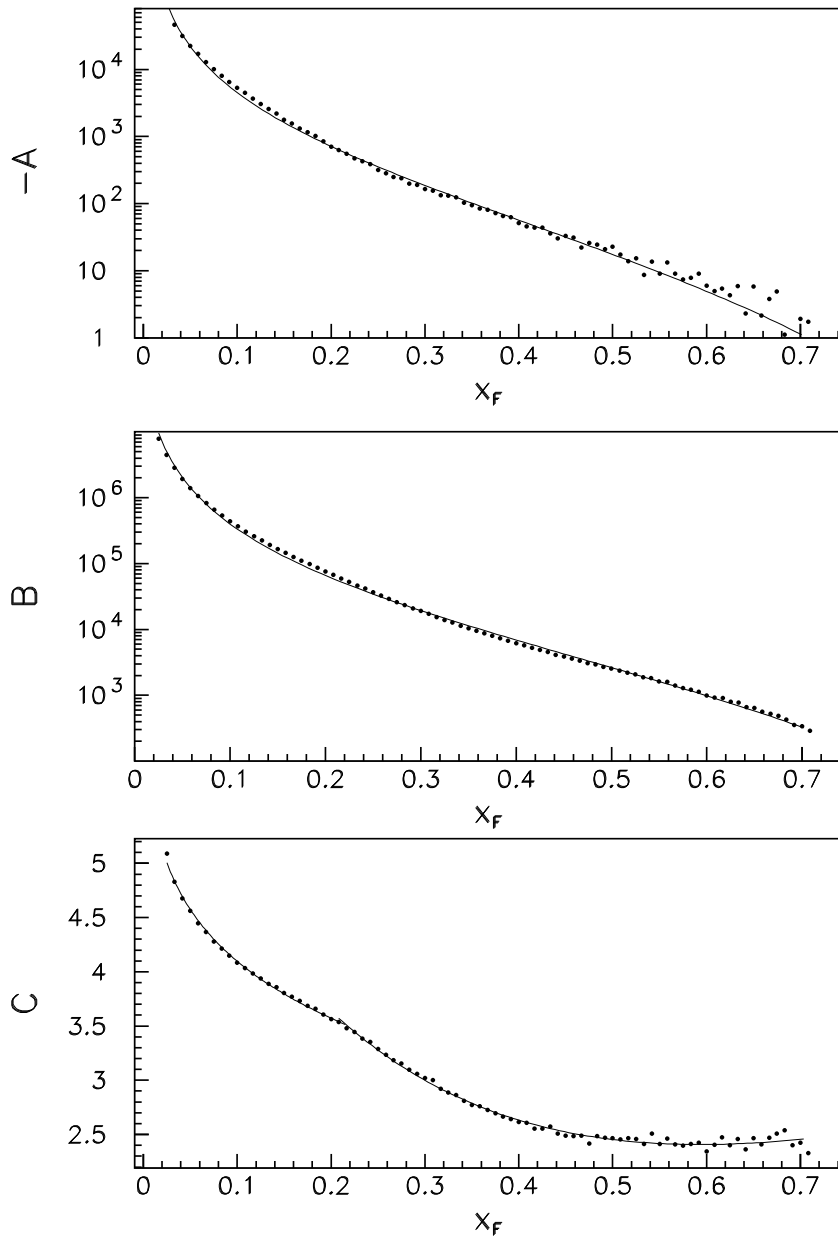


Figure 8: The points are the coefficients A , B , and C obtained when fitting Figure 6 to Equation 1. The curves are the fit of these points to the functions $A(x_F)$, $B(x_F)$, and $C(x_F)$ from Equation 2.

4 Fit to ND data

The fit to the ND data uses the ν_μ and $\bar{\nu}_\mu$ spectra from 7 different beam configurations (LE010z000, LE010z170i, LE010z185i, LE010z200i, LE100z200i, LE150z200i and LE250z200i). There are two data sets in LE250z200i configurations taken in 2005 and 2006. Both data sets are used. Since one was taken in the early running at low intensity, it requires a correction due to beam width [2]. Neutrinos of all energies (0-120GeV) are included into the fit.

We use 16 parameters to tune the hadron production. Five parameters are used for other beam related systematics and there are 5 other non-beam related parameters. In total 26 parameters are used in the fit.

The ν_μ histograms all have 70 energy bins, while in case of $\bar{\nu}_\mu$ the number of bins depends on the beam configuration: the LE010z185i $\bar{\nu}_\mu$ has the most events, so 70 bins were used, while the other $\bar{\nu}_\mu$ histograms were binned with 29 bins.

The fits were done using two different selection algorithms for selecting charged-current (CC) ν_μ s in MINOS: the RO PID [11] and DP PID [12]. We tried both to ensure there were no significant detector effects in the flux determination. For $\bar{\nu}_\mu$ data and MC, only the RO PID [11] selection was used.

4.1 Hadron production parameters

Of 16 parameters that are used for hadron productions, 6 are for π^+ , 6 for K^+ and then 2 for π^- and 2 for K^- . Figure 2 shows the MC simulation of ND spectrum for different beam configurations broken by neutrino parent. It can be seen that the high energy part of the spectrum comes mostly from kaons, while the low energy part comes predominantly from pions.

As the sensitivity in $x_F - p_T$ space is larger for positive mesons than for negatives, we use more parameters for positives. The 6 parameters used for π^+ redefine the $A(x_F)$, $B(x_F)$ and $C(x_F)$ that were defined in Section 3:

$$A'(x_F) = (par[0] + par[1] \cdot x_F)A(x_F)$$

$$B'(x_F) = (par[2] + par[3] \cdot x_F)B(x_F)$$

$$C'(x_F) = (par[4] + par[5] \cdot x_F)C(x_F)$$

Similarly par[6] through par[11] are used to redefine the $A(x_F)$, $B(x_F)$ and $C(x_F)$ parameters for K^+ . The weight for a meson is calculated using:

$$W(p_{type}, p_T, x_F) = \frac{[A' + B'p_T] * \exp(-C'p_T^{3/2})}{[A + Bp_T] * \exp(-Cp_T^{3/2})} \quad (3)$$

Because we use this ratio, the method does not critically depend on how well the parameterization fits the Fluka 2005 distributions of Figures 6 and 7.

The target yield ratios such as π^+/π^- and K^\pm/π^\pm are somewhat well-constrained by experimental data and by theoretical expectations. We constrain the π^- (K^-) weights to take on the same values as the π^+ (K^+) weights, up to a linear correction in x_F :

$$W(\pi^-, p_T, x_F) = (\text{par}[12] + \text{par}[13] \cdot x_F)W(\pi^+, p_T, x_F)$$

$$W(K^-, p_T, x_F) = (\text{par}[14] + \text{par}[15] \cdot x_F)W(K^+, p_T, x_F)$$

Using the same initial weights preserves the ratios π^+/π^- and K^\pm/π^\pm to first order since the p_T distributions are very similar for positive and negative mesons.

We don't have sensitivity to K_L^0 when fitting the muon type neutrinos, but their production is important for flux of electron type neutrinos. The weight for K_L^0 is calculated using the weights for positive and negative kaons. We follow the prescription given in [18]. Using the simple parton model and assuming the isospin symmetry gives us $u_v/d_v = 2$, $u_s = \bar{u}_s = d_s = \bar{d}_s$ and $s_s = \bar{s}_s$ where q_v are valence quarks and q_s are sea quarks. The number of K_L^0 ; $N(K_L^0) = N(K_S^0)$ is related to $N(K^+)$ and $N(K^-)$ through:

$$N(K_L^0) = \frac{N(K^+) + (2n - 1)N(K^-)}{2n}$$

where $n = u/d$ and in this simple model $n=2$, so we have:

$$N(K_L^0) = \frac{N(K^+) + 3N(K^-)}{4}$$

This model agrees with K_S production within 15% up to $x_F = 0.5$. At higher x_F , the dependence of n on x_F becomes important.

To constrain the fit, penalty terms are applied on the $\langle p_T \rangle$ of particles and on the ratios π^+/π^- and K^\pm/π^\pm . The spread of $\langle p_T \rangle$ predicted by different hadron production models (see Table 1) motivates a penalty term of 15 MeV in $\langle p_T \rangle$. The spread in π^+/π^- and K^\pm/π^\pm (see Figures 17 and 18) motivate penalty terms of 20% on these quantities. In all cases, we are taking Fluka2005 as the ‘‘central value’’ about which we allow the fit to deviate.

4.2 Beam parameters

The effect of various beam related systematics (non hadron production) on the neutrino spectrum and estimated size of the uncertainty for each of the systematic is documented in [2]. Five systematics that have the most noticeable effect on the near detector spectrum are used in the fit:

- Horn 1 Offset ($1\sigma \equiv 1$ mm)
- Baffle scraping ($1\sigma \equiv 0.25\%$)
- POT uncertainty ($1\sigma \equiv 2\%$)

- Horn Current Miscalibration ($1\sigma \equiv 1\%$)
- Horn Current Distribution ($1\sigma \equiv$ difference between $\delta = \text{inf}$ and $\delta = 6\text{mm}$)

Values noted in parentheses are the estimated uncertainties and those were used as penalty terms in the fit.

4.3 Other parameters

Five additional parameters are used to account for some detector effects and $\bar{\nu}_\mu$ cross sections:

- ν energy miscalibration ($1\sigma \equiv 5\%$)
- Shower offset ($1\sigma \equiv 50$ MeV)
- NC for ν_μ ($1\sigma \equiv 30\%$)
- NC for $\bar{\nu}_\mu$ ($1\sigma \equiv 30\%$)
- $\bar{\nu}_\mu$ cross section ($1\sigma \equiv 30\%$)

Values noted in parentheses are the estimated uncertainties and those were used as penalty terms in the fit.

The cross section parameter was used to change the $\bar{\nu}_\mu$ cross sections only below 25 GeV, reflecting the greater uncertainties at lower neutrino energies. A functional form that was used to reweight for cross sections was such that it smoothly approaches 1 at 25 GeV and was exactly equal to 1 above 25 GeV where $\bar{\nu}_\mu$ cross sections are well known.

4.4 Corrections to MC

Since the data in LE100z200i and LE250z200i configurations from 2005. was taken with low intensity beam that was narrower profile than the beam width that is used in MC simulations, a correction to the MC is applied. Further discussion about the spot size corrections can be found in [2].

The newest LE010z185 data is taken with new target and baffle assembly. The exact position of this target is not yet known precisely and it can be a centimeter off. We don't use the new data in the fit, but we find the correction due to the target z position by fitting the new data using the best fit parameters and adding the additional parameter for target z position. Such will be the subject of a forthcoming note.

4.5 Results of the fit

Figures 10 through 13 show the results of the fits using Rustem's PID. Table 3 summarizes the χ^2 s. For comparison χ^2 s from the previous fits using Birch reconstruction and Carrot MC are also listed. Note that compared to the fits done with Birch/Carrot ntuples 6 additional data

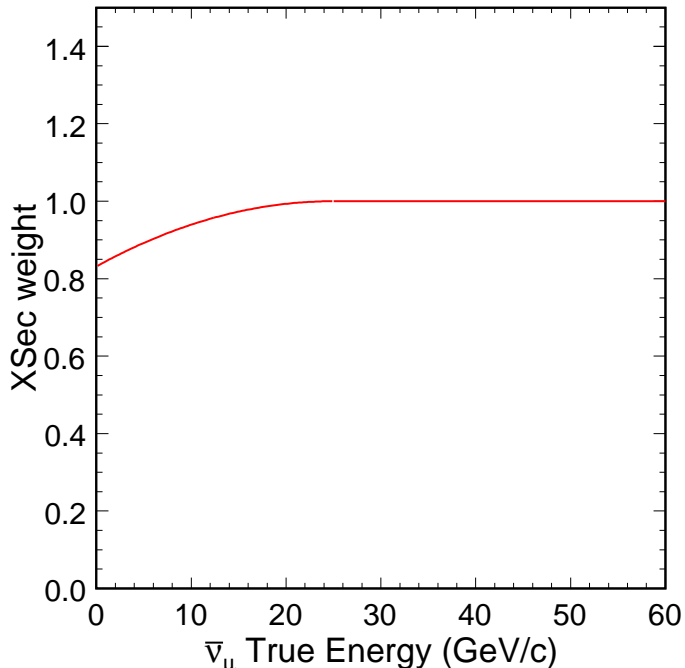


Figure 9: The fit allows $\bar{\nu}_\mu$ cross sections to change below 25GeV. The plot shows the weight that comes out of the fit depending on the $\bar{\nu}_\mu$ true energy.

histograms were used for the Cedar/Daikon fit (ν_μ LE150/200kA and new LE250/200kA; $\bar{\nu}_\mu$ LE10/170kA, LE10/200kA, LE150/200kA and new LE250/200kA).

Table 3 also lists the χ^2 s for a fit that was done using David’s PID and Cedar/Daikon ntuples. Using different PID selection didn’t affect the fit too much. The χ^2 s and the fit parameters came out very close for the two selections, which is encouraging.

Table 4 lists the fit parameters. Figure 9 shows the pull on the $\bar{\nu}_\mu$ cross section. The “DP” and “RO” PID selections yield similar fit parameters. All of the beam-related fit parameters are within a “sigma” of their nominal values, and are consistent between the two PID selections. The only noticeable difference is for the ν_μ NC contamination, which requires adjustment using the DP PID by $(24 \pm 4)\%$, and is consistent with no adjustment, $(2 \pm 7)\%$, in the RO PID.

Figures 14 through 16 show the adjustments necessary to the particle production (weights, p_T spectra, etc) in order to fit the ND data. Figures 17 and 18 show the effect of the fit on some of the external constrains. For the K/π ratio, for example, the fit was able to choose a value close to the Fluka2005 spectrum, and within a disagreement at the level of the model spread. The sole quantity pulled very hard toward the ND data is the π^+/π^- ratio. As can be seen this quantity had to be pulled significantly away from the Fluka2005 curve. Interestingly, however, our data suggest a π^+/π^- ratio that is quite similar to recent results from NA49[10]. This is significant because the NA49 data was not used in the fit. Although

the NA49 data is for thin Carbon targets, the fraction of pions arising from secondary interactions in the target is only $\approx 10\%$ for $x_F > 0.5$, so the NA49 data is of relevance to MINOS. In fact, it might be sensible in the future to use this data or MIPP data as our external constraint, rather than the Fluka2005 ratios.

Beam Configuration	Fit χ^2 (statistical errors only)/NDF	
	No Tuning RO(DP)	This Fit
ν_μ LE10/000kA	1042 (1033)/70	146 (166)
ν_μ LE10/170kA	588 (581)/70	84 (84)
ν_μ LE10/185kA	1440 (1419)/70	84 (83)
ν_μ LE10/200kA	587 (606)/70	64 (64)
ν_μ LE100/200kA	1441 (1336)/70	199 (181)
ν_μ LE150/200kA	1205 (1135)/70	109 (128)
ν_μ LE250/200kA ^(a)	699 (661)/70	93 (81)
ν_μ LE250/200kA ^(b)	778 (734)/70	50 (45)
$\bar{\nu}_\mu$ LE10/000kA	119/28	50 (46)
$\bar{\nu}_\mu$ LE10/170kA	107/28	47 (45)
$\bar{\nu}_\mu$ LE10/185kA	459/68	90 (89)
$\bar{\nu}_\mu$ LE10/200kA	58/28	32 (36)
$\bar{\nu}_\mu$ LE100/200kA	114/27	73 (75)
$\bar{\nu}_\mu$ LE150/200kA	72/28	29 (26)
$\bar{\nu}_\mu$ LE250/200kA ^(a)	67/28	43 (40)
$\bar{\nu}_\mu$ LE250/200kA ^(b)	70/28	39 (41)
Penalty terms		109 (123)
Total (all beams)	=10.8	(1351/794=1.7)
^(a) 2005 data	^(b) 2006 data	

Table 3: Comparison of χ^2 s between data and MC before and after tuning. Previous fits done with Birch/Carrot ntuples are shown for comparison. Cedar/Daikon fits were done with two different selections for ν_μ s. One using Rustem's PID (RO) and the other using David's PID (DP).

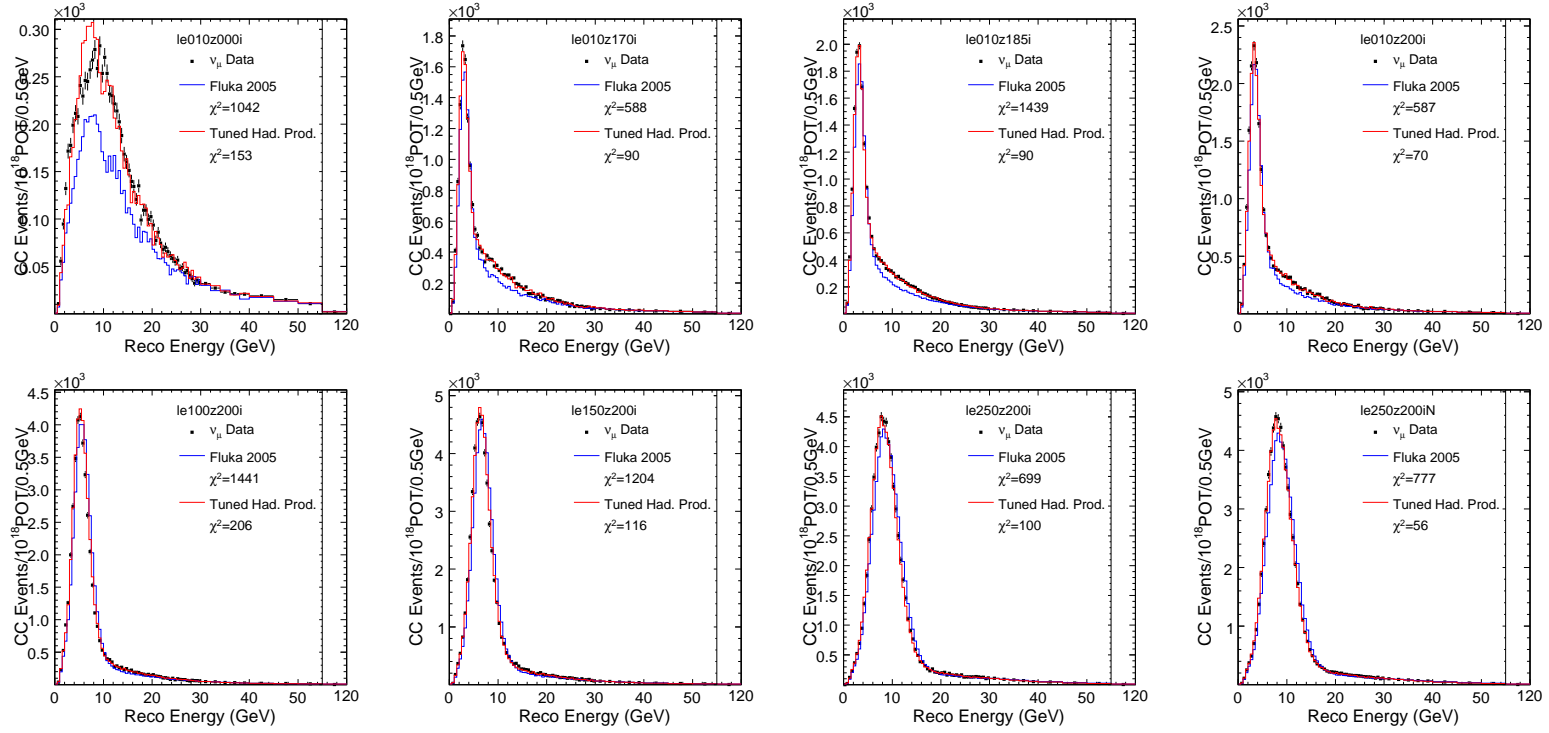


Figure 10: The ND ν_μ CC data (black points) have been selected using Rustem's PID. The blue curves are the MC before tuning, the red is the MC after tuning.

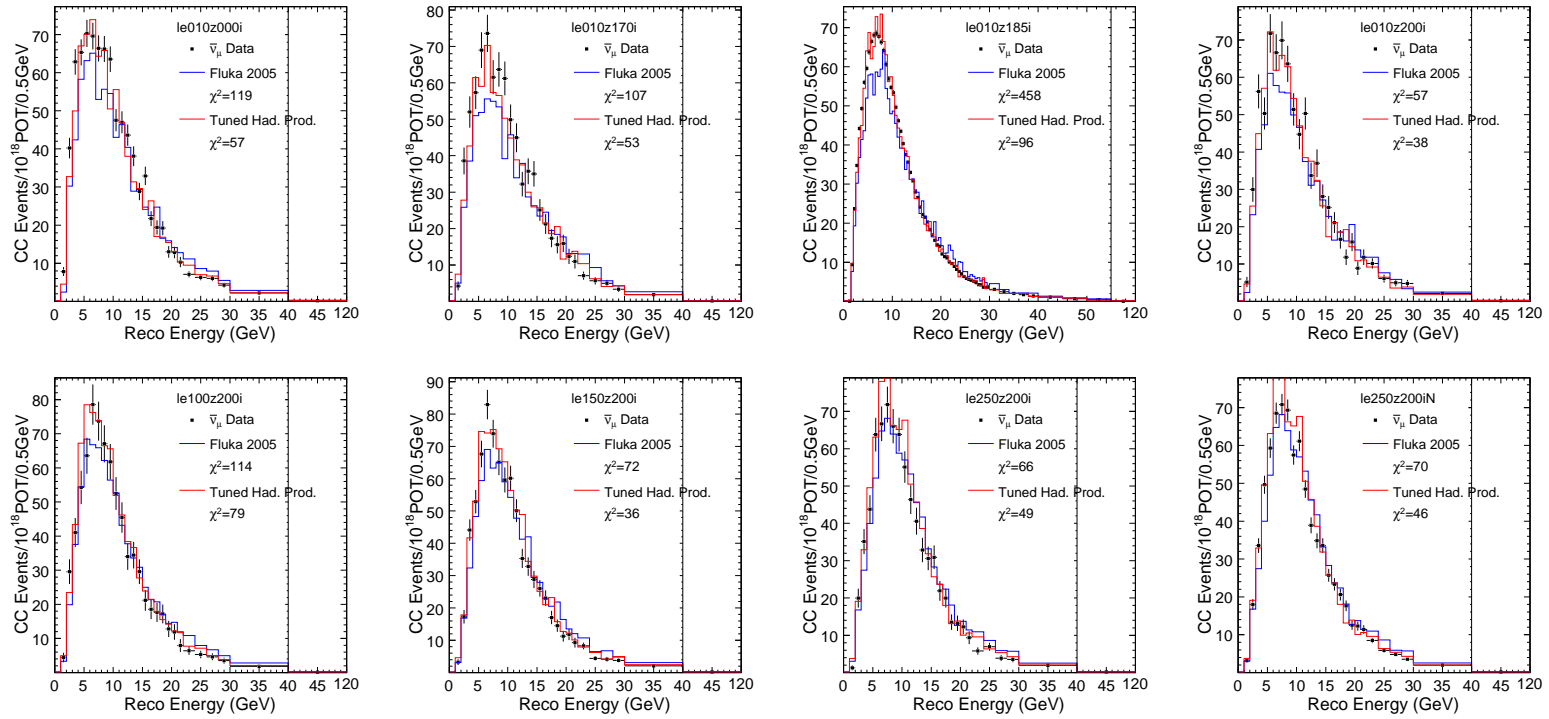


Figure 11: Black points are $\bar{\nu}_\mu$ ND CC data. The blue curves are the MC before tuning, the red is the MC after tuning.

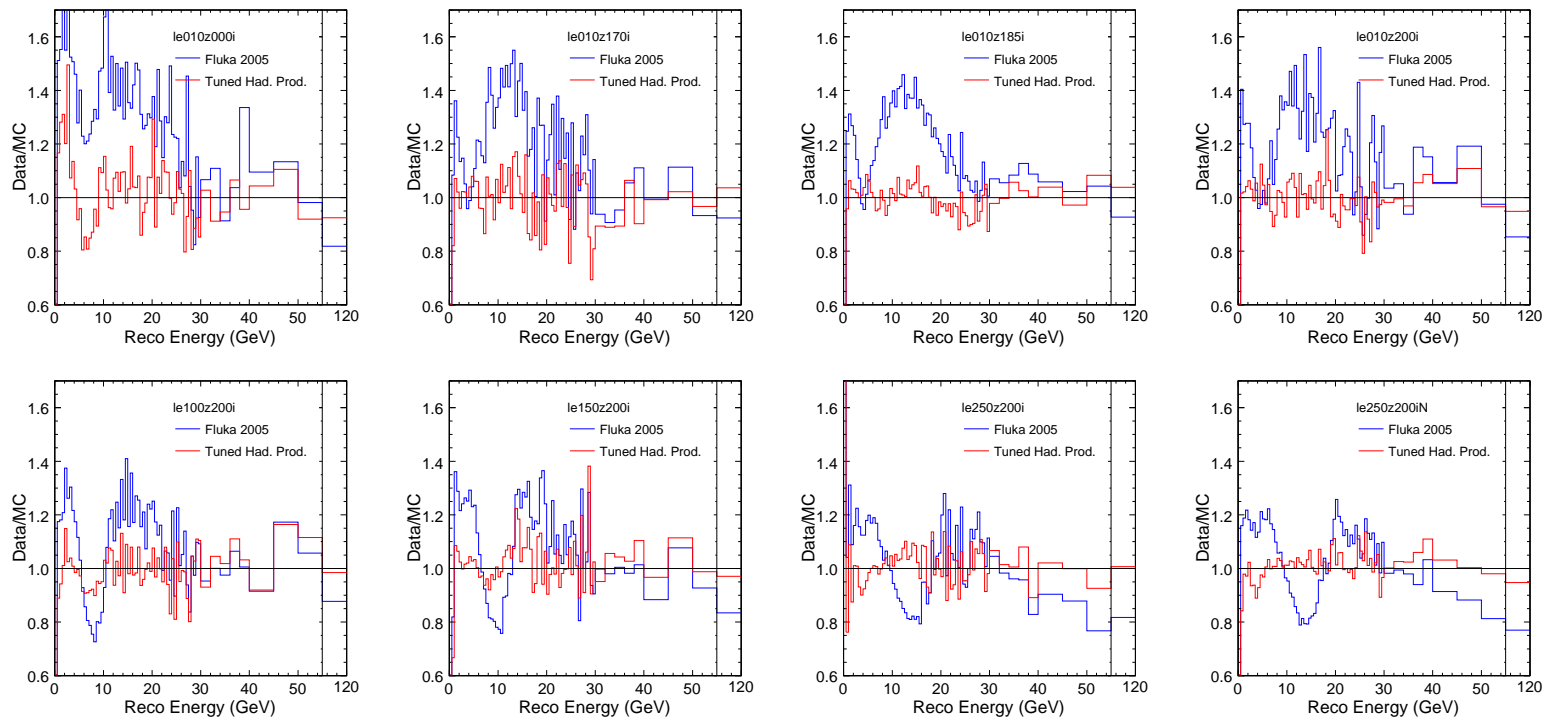


Figure 12: ν_μ Data/MC ratio plots using Rustem's PID. The blue curves are the MC before tuning, the red is the MC after tuning.

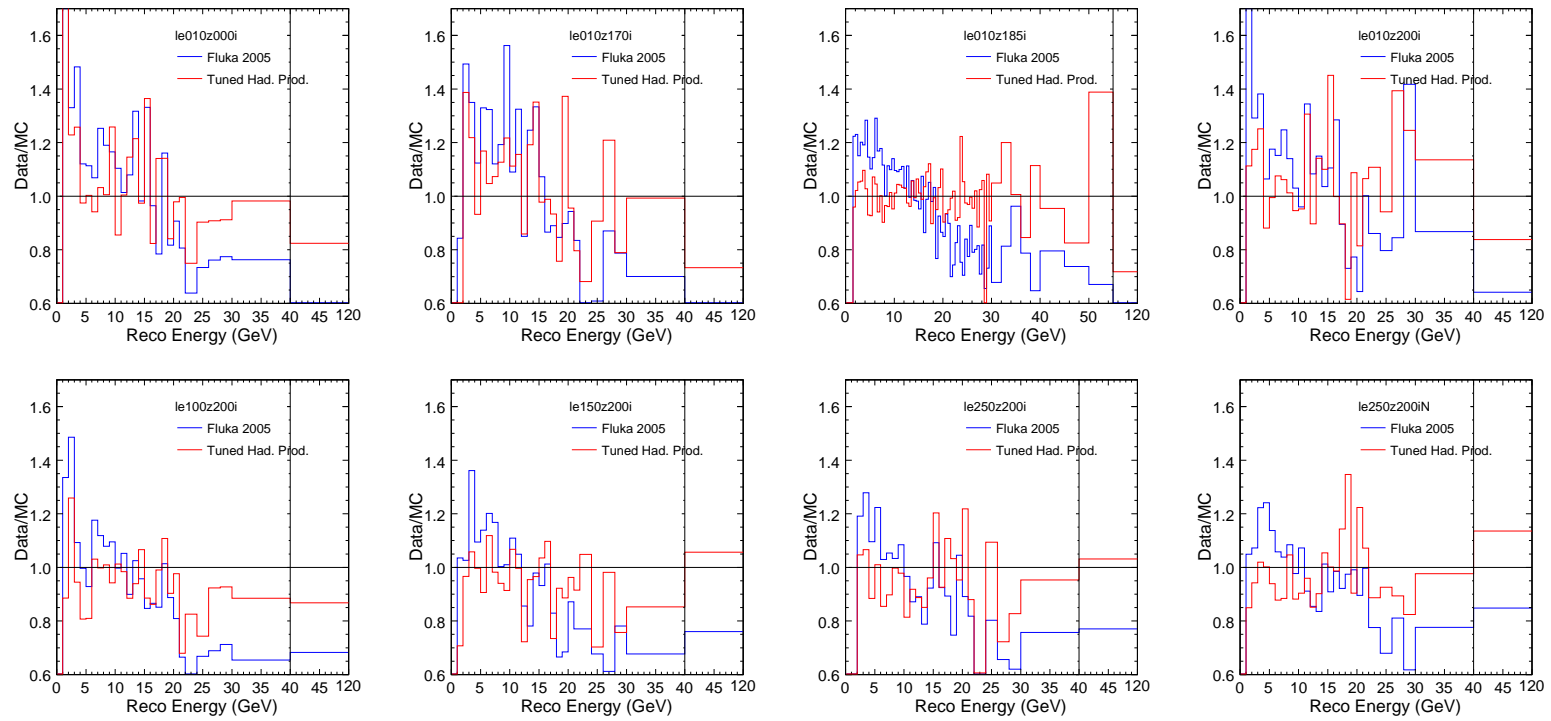


Figure 13: Data/MC ratio plots for $\bar{\nu}_\mu$. The blue curves are the MC before tuning, the red is the MC after tuning.

	RO		DP	
	Parameter	Error	Parameter	Error
Horn 1 Offset	-0.58	0.22	-0.58	0.22
Baffle Scraping	0.29	0.24	0.27	0.24
POT	0.02	0.20	0.00	0.22
Horn Current Miscalibration	-0.24	0.15	-0.43	0.16
Horn Current Distribution	-0.26	0.15	-0.43	0.17

Table 4: Results of the fit for various beam systematic parameters. The entries in the table are the number of “sigma” by which a given parameter must be adjusted to obtain agreement with the ND data. Fits using two different PID selections for ν_μ s are shown. Both fits use the same $\bar{\nu}_\mu$ selection.

	RO		DP	
	Parameter	Error	Parameter	Error
Energy miscalibration / %	5.7	0.	5	0.
Shower offset / MeV	11	0.	-13	0.
NC ν_μ / %	2	7	25	4
NC $\bar{\nu}_\mu$ / %	5	7	6	7
$\bar{\nu}_\mu$ xsec	0.83	0.02	0.82	0.02

Table 5: The best fit values for five parameters used in addition to 21 beam related parameters. Fits using two different PID selections for ν_μ s are shown. Both fits use the same $\bar{\nu}_\mu$ selection.

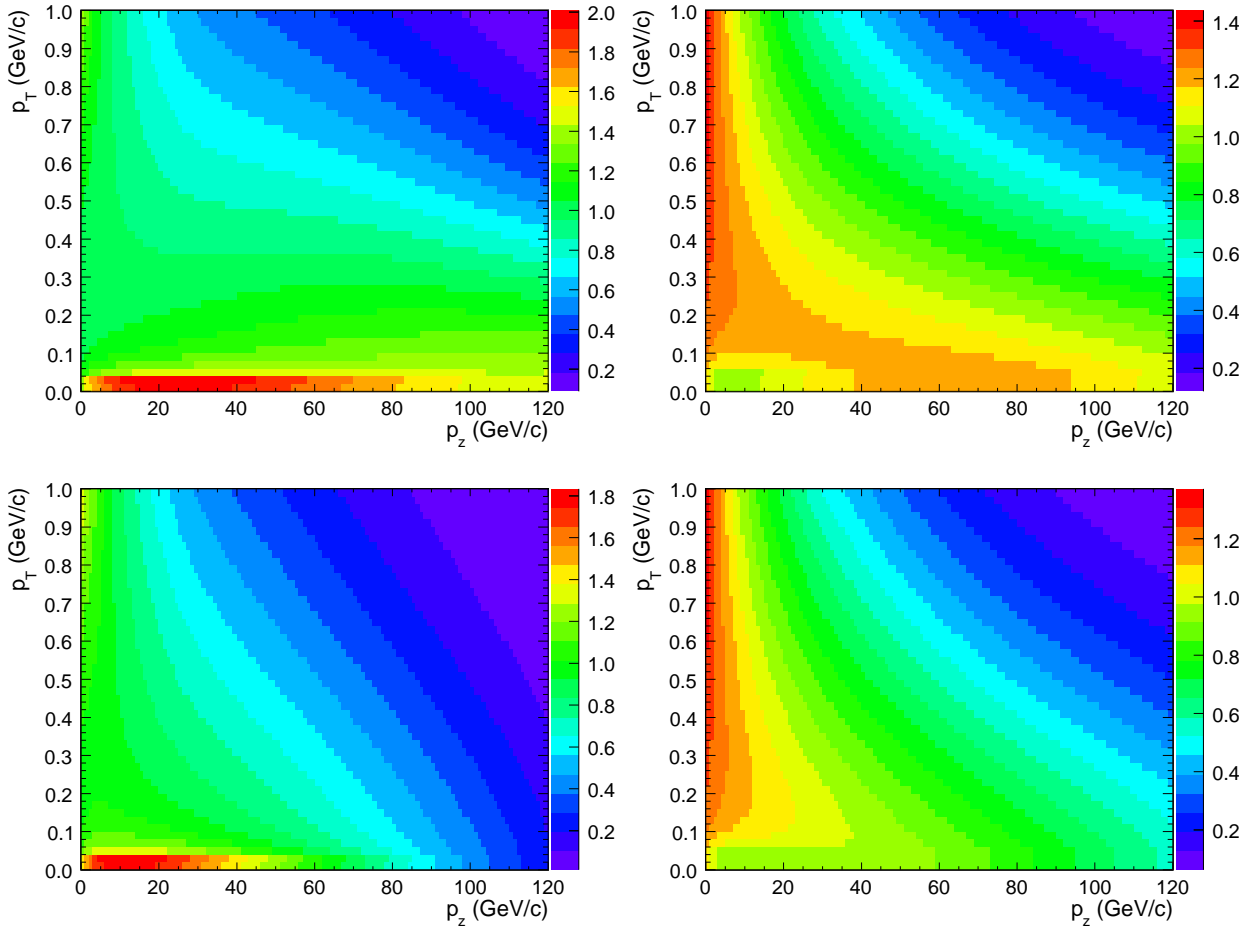


Figure 14: The weights that should be applied to secondaries leaving the target depending on their longitudinal momentum (p_z) and transverse momentum (p_T) to achieve better agreement between MC and Near Detector data. Top left is for π^+ , top right for K^+ , bottom left for π^- and bottom right for K^- .

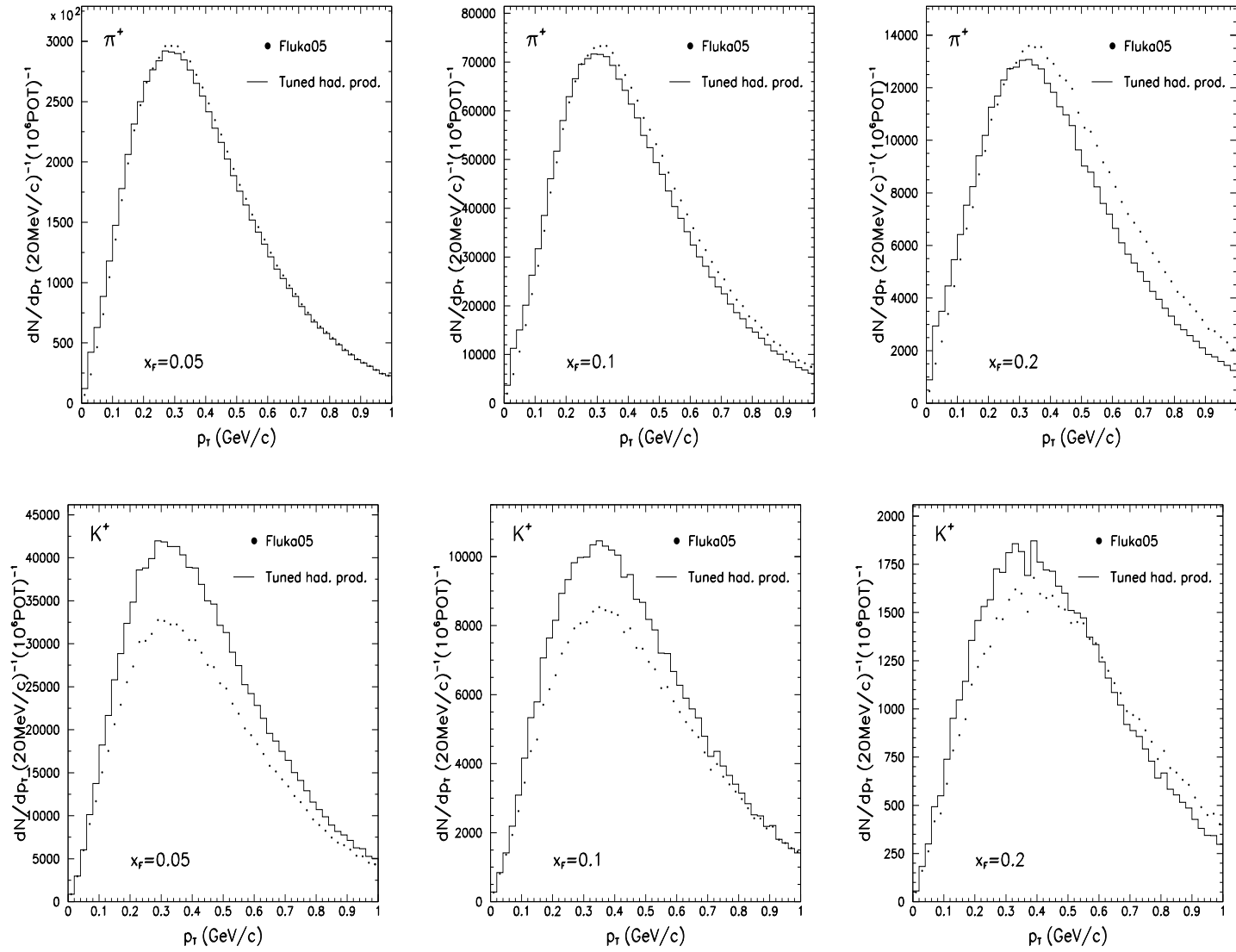


Figure 15: Effect on primary hadron distributions. Shown are the p_T distribution of positive pions and kaons at three different values of x_F (*i.e.*: subsets of the pion and kaon distribution in Figure ??).

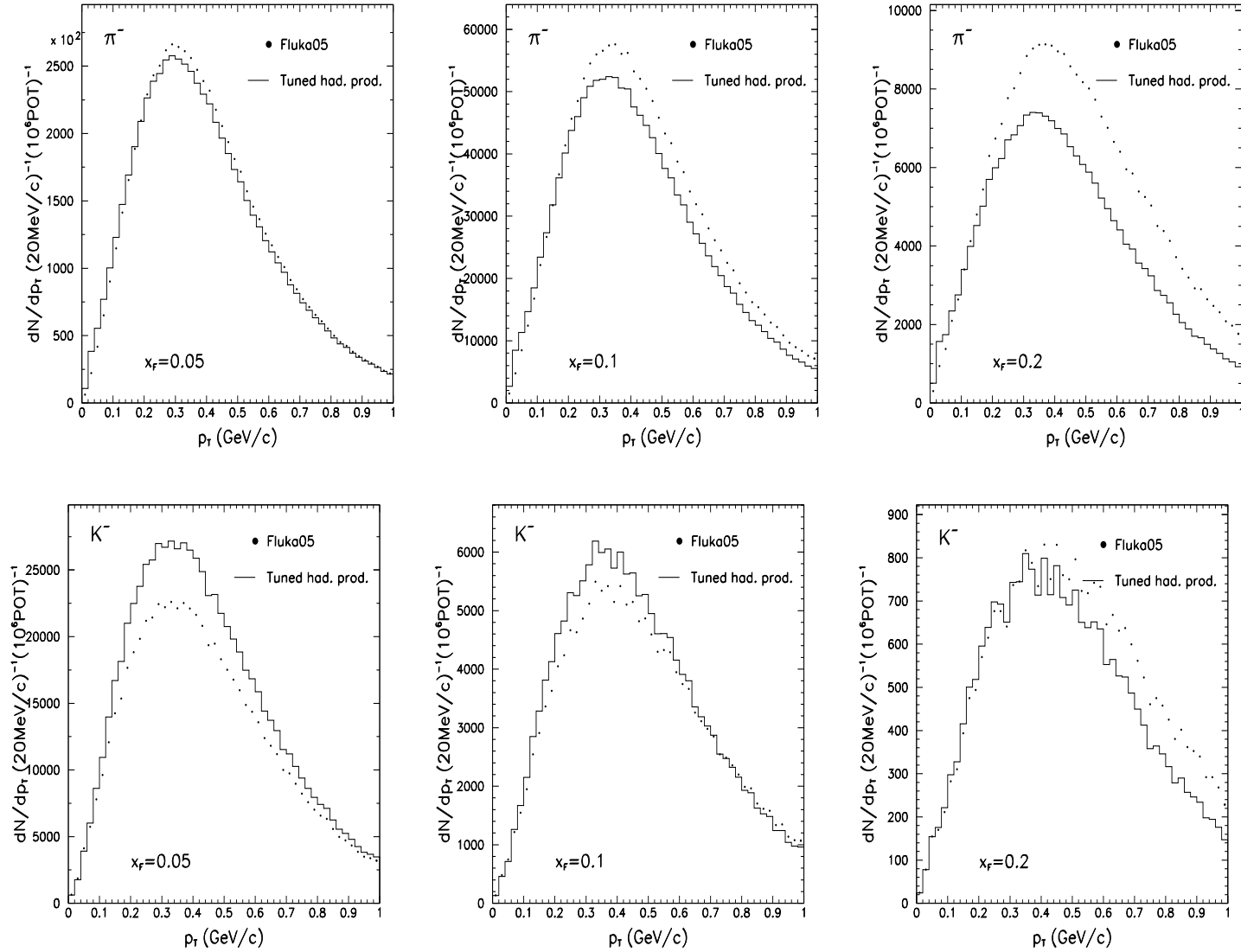


Figure 16: Effect on primary hadron distributions. Shown are the p_T distribution of negative pions and kaons at three different values of x_F (*i.e.*: subsets of the pion and kaon distribution in Figure ??).

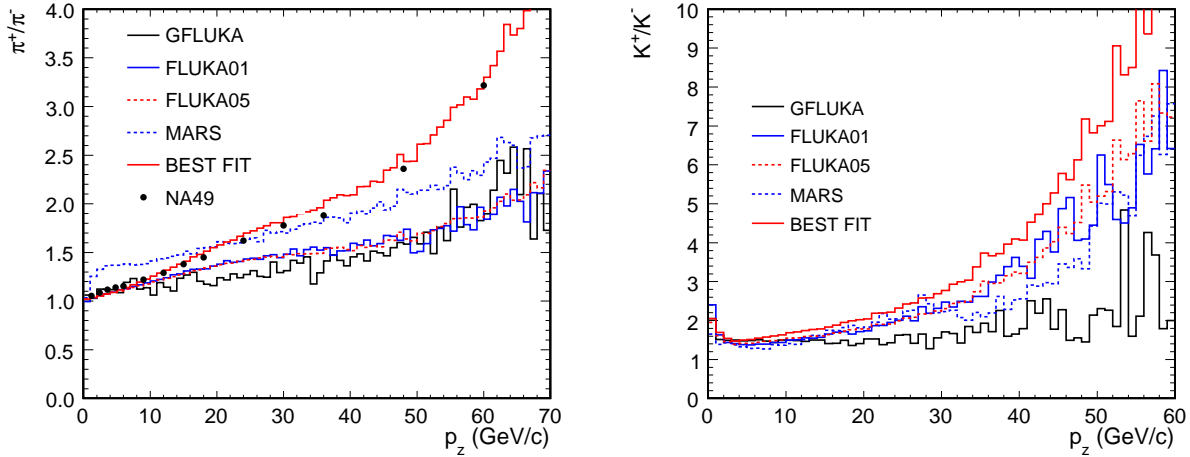


Figure 17: Left plot shows π^+/π^- ratio and right plot shows k^+/k^- before and after MC tuning. Prediction from few other hadron production models are shown for comparison. NA49 data is shown on the π^+/π^- ratio plot. Tuning the MC pulls the nominal Fluka 2005 ratio toward the NA49 data.

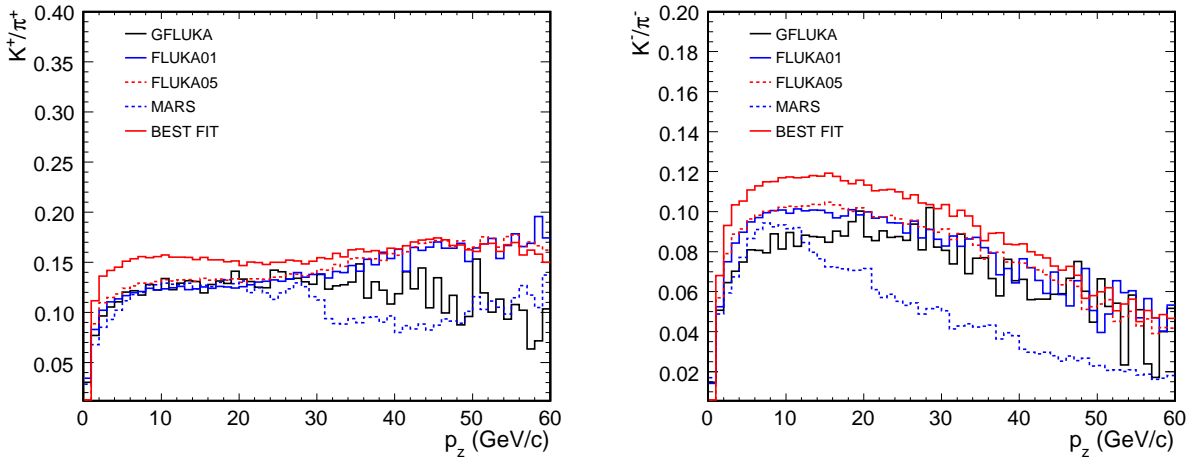


Figure 18: k/π ratios for before and after the MC tuning. For comparison ratios from different hadron production models are also shown. Left plot is for positives and right for negatives.

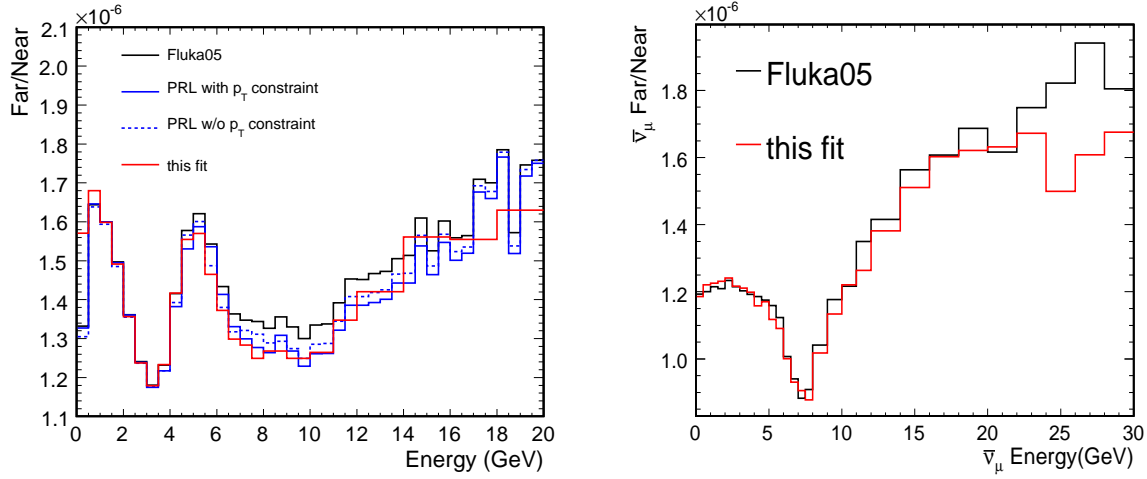


Figure 19: Comparison of the far over near ratio before and after the fit. Left plot is for ν_μ and right for $\bar{\nu}_\mu$.

5 Hadron Production Uncertainty After Tuning

It is expected that the fitting procedure will reduce the uncertainty on the Near detector flux. Some residual uncertainty remains due to the statistical uncertainty on the fitted parameters. Here we evaluate the remaining Hadron production uncertainty after the fit by varying the 16 hadron production parameters within 1σ from their best-fit values determined from MINUIT.

We generate 750 sets of parameters and reweight the MC with each set. For each energy bin, the maximal deviation from the “nominal” spectrum was taken as the uncertainty. Here we assume that the “nominal” spectrum is the one we get by reweighting the MC using the best fit parameters.

Some of the hadron production parameters are correlated and that was taken into account when generating different sets of parameters.

Figures 20 and 21 show the errors for ND spectrum and the for 6 different beam configurations both for neutrinos and anti neutrinos.

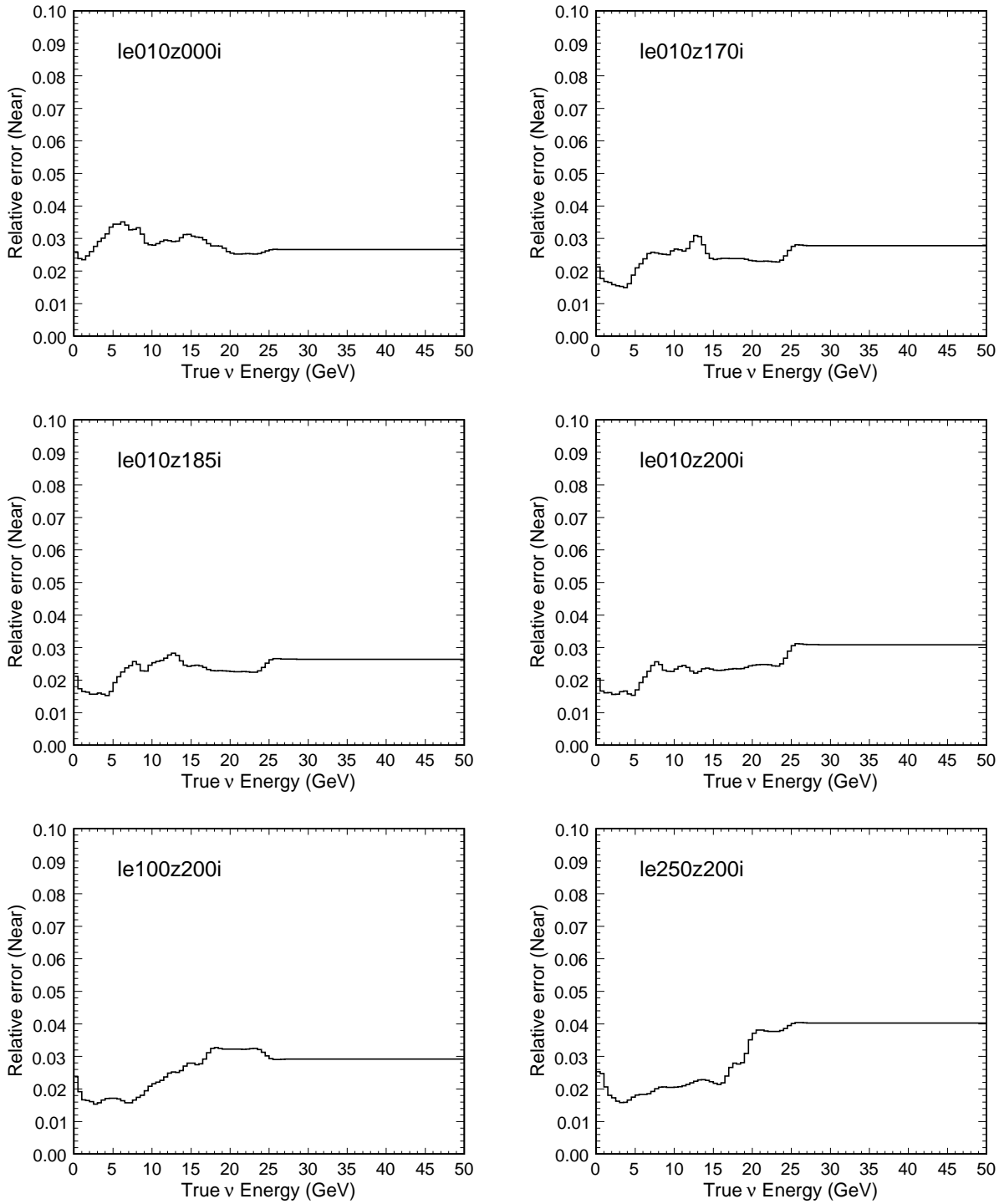


Figure 20: ν_μ uncertainty in Near Detector spectrum due to hadron production uncertainty. Shown is the remaining uncertainty after the fit to Near Detector data

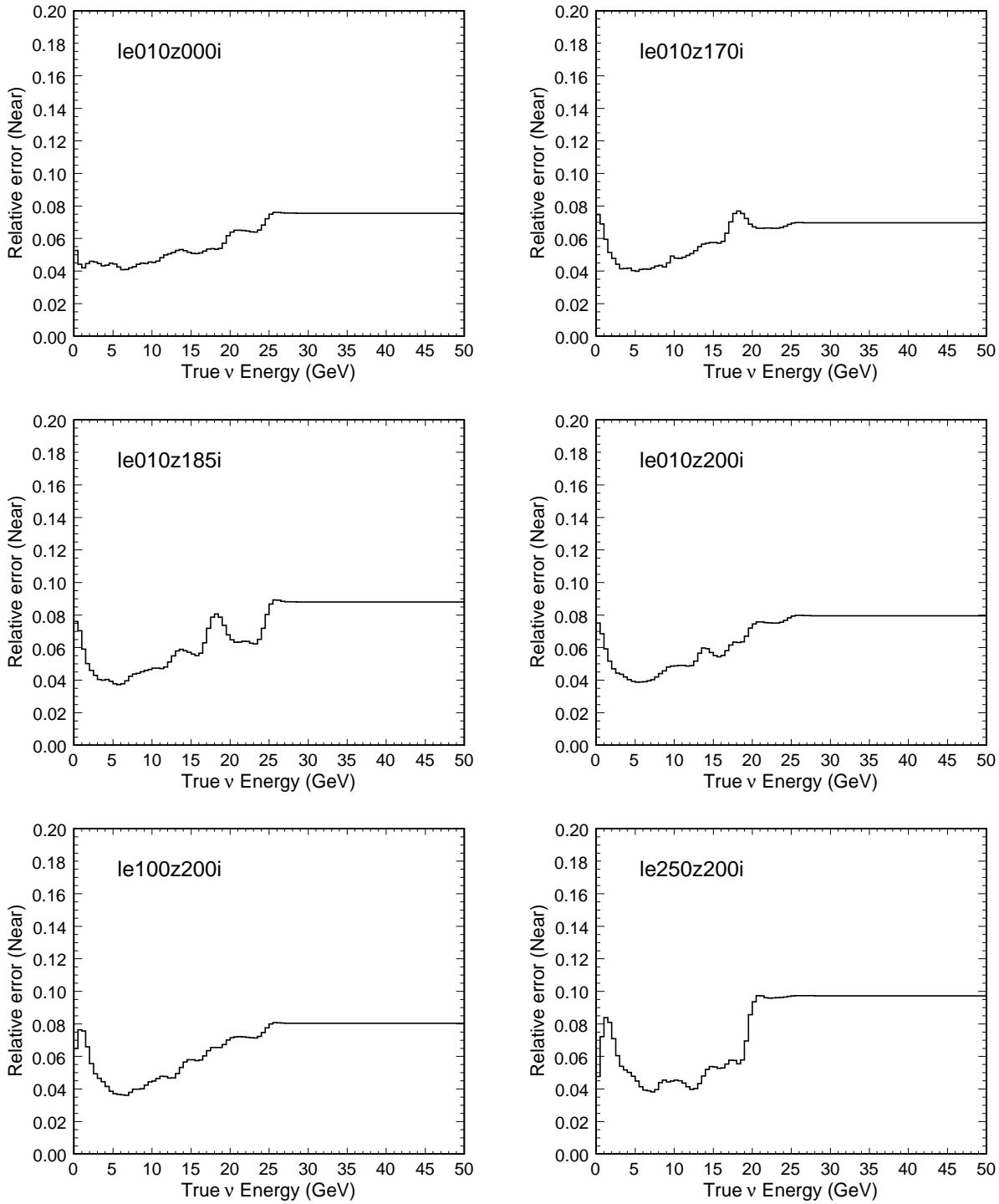


Figure 21: $\bar{\nu}_\mu$ uncertainty in Near Detector spectrum due to hadron production uncertainty. Shown is the remaining uncertainty after the fit to Near Detector data.

6 Impact on ν_e Flux

The same hadrons whose decays lead to ν_μ and $\bar{\nu}_\mu$ events also lead to ν_e and $\bar{\nu}_e$. Figure 22 shows the p_T and p_z of hadrons which contribute to the ν_e or $\bar{\nu}_e$ fluxes. The π^\pm contributions are from $\pi \rightarrow \mu\nu_\mu \rightarrow (e\nu_\mu\nu_e)\nu_\mu$ decays in which the tertiary muon leads to the ν_e (likewise for the K^\pm), while the K_L contribution is largely from K_{e3} decays. Since the muon lifetime is long, only the slow π^\pm and K^\pm decays lead to ν_e events. Thus, the spectra in Figure 22 are quite similar to Figures 4 and ??, but truncated at large p_z . It may be therefore expected that the ν_μ fits can serve to constrain the ν_e flux as well.

As of this time, we have not performed an explicit fit to the observed $(\nu_e + \bar{\nu}_e)$ spectrum in the ND. As can be seen in Figure 23, the $(\nu_e + \bar{\nu}_e)$ is dominated by the $\pi \rightarrow \mu \rightarrow \nu_e$ decay chain at low E_ν , with a long tail due to K_L and K^\pm decays. Because the pion parents are fairly well-constrained (at the level of 5%), by the ν_μ and $\bar{\nu}_\mu$ spectra, it is largely sufficient for $(\nu_e + \bar{\nu}_e)$ background prediction for the oscillation search. At high E_ν , the charged kaon component is likewise well-constrained, though the K_L component is not. Thus, an explicit fit to the ND $(\nu_e + \bar{\nu}_e)$ under investigation by J. Boehm and will be helpful in the future.

Figure 23 shows the effect of the hadron production tuning presented in the previous sections on the $(\nu_e + \bar{\nu}_e)$ spectrum in the LE010/185kA beam. Not surprisingly, since the LE010/185kA event rate for ν_μ 's was only pulled by $\sim 10\%$ (averaging over neutrino energies), the $(\nu_e + \bar{\nu}_e)$ spectrum shows only a small effect.

Figure 24 shows the anticipated spectrum and F/N errors for the ν_e search from hadron production using the same procedure as in the previous section for ν_μ 's. For the present time, we have ascribed a 50% error on the K_L yields, since these are poorly-constrained by the ν_μ 's.

7 Conclusions

The present analysis allows users to reweight the beam MC flux to force agreement with the ND data. We found that the hadron production model can readily be tuned within its allowed range to simultaneously describe well the various beam configurations. This serves as a powerful demonstration of our understanding of the beam and the ability to describe up to 30% discrepancies in the ND data. Because of the several configurations available in the NuMI beam, we are able to disentangle various effects which are measured in the $(\text{flux}) \times (\text{cross-section}) = (\text{event rate})$.

We wish to emphasize that the hadron reweighting exercise performed in this note is sensitive to only portions of the (x_F, p_T) plane. We are NOT very sensitive, for example, to the region $p_T > 500$ MeV. Thus, in trial fits in which we let the hadron production parameters vary freely, or fits in which we constrain $\langle p_T \rangle$ to stay within 20-30 MeV of the nominal Fluka2005 value, we were able to get acceptable fits with similar χ^2 with or without the $\langle p_T \rangle$ constraint. While we feel confident that we have produced a beam tuning that is stable, and whose effect on the flux is well-understood, we do not intend to promote this analysis as a measurement of the underlying physics distributions. The invariant quantity

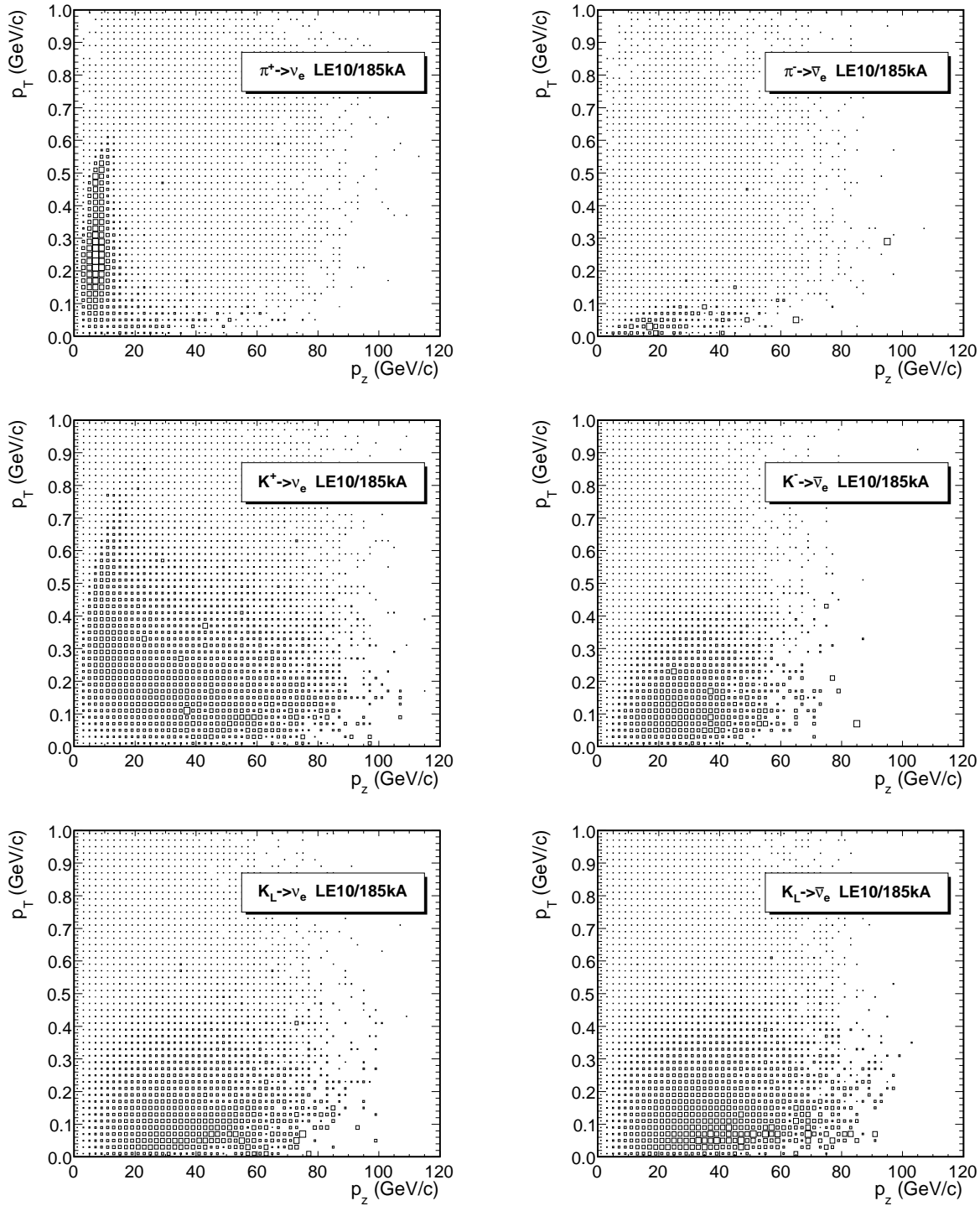


Figure 22: The p_z and p_T of hadrons off the target which contribute to the ν_e (left column) or $\bar{\nu}_e$ (right column) fluxes. Shown are the contributions for charged pions (top row), charged kaons (middle row), and K_L (bottom row).

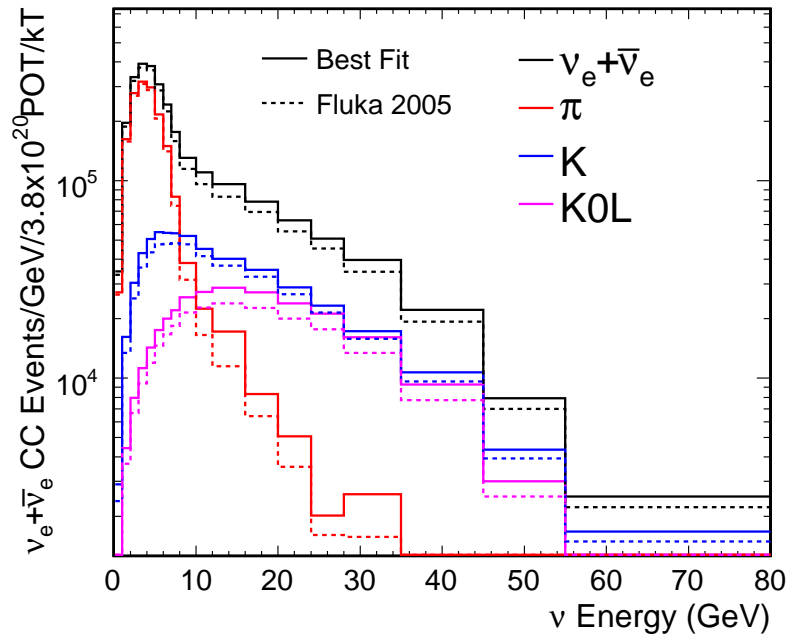
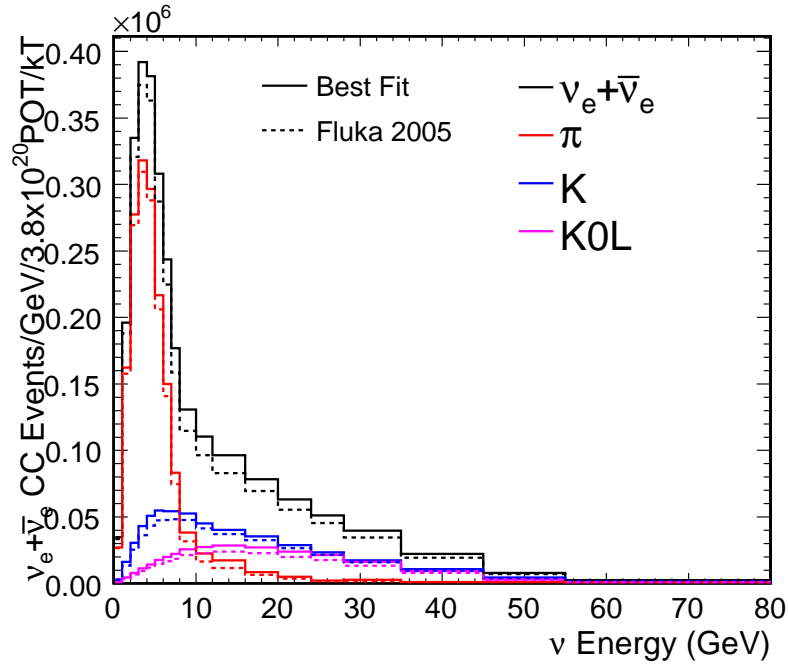


Figure 23: Sum of ν_e and $\bar{\nu}_e$ event rates in the ND. The contributions from K^\pm (blue curve), K_L (pink curve) and π^\pm (red curve), as well as the total event rate (black curve), are shown. Dashed curves are for the beam MC with Fluka 2005 hadron production model, while the solid curves show the beam MC after the tuning to the ν_μ and $\bar{\nu}_\mu$ spectra from the previous sections.

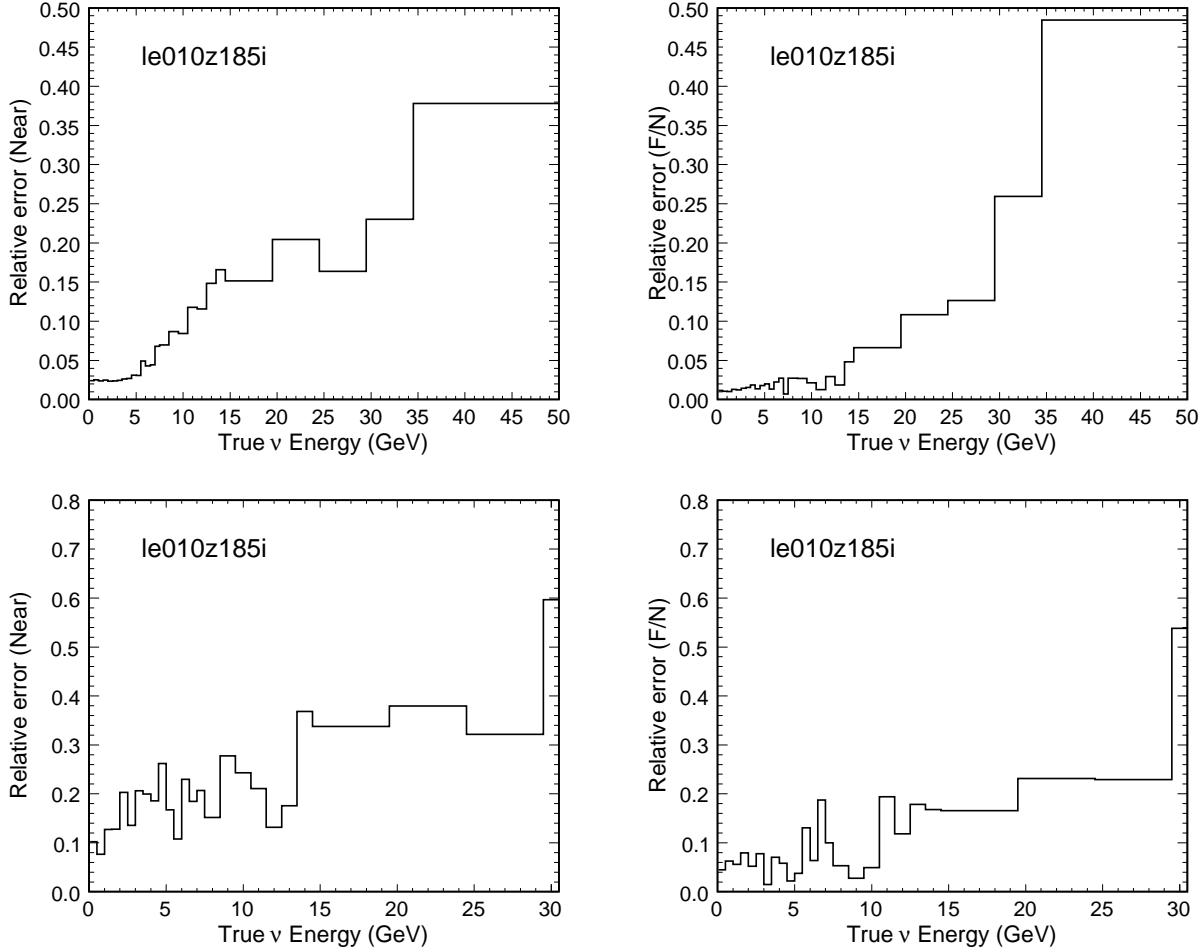


Figure 24: Errors due to hadron production for ν_e (top row) and $\bar{\nu}_e$ (bottom row). The errors are for the ND event rate (left column) and F/N ratio (right column). Because the K_L spectrum off the target is not well constrained by the ν_μ and $\bar{\nu}_\mu$ fluxes, we have ascribed at 50% uncertainty in the K_L yields, leading to substantial spectrum and F/N uncertainties at high E_ν .

derived from this analysis is not the underlying hadron distributions, but rather the flux, which is found to be modified by this analysis, but stable to $< 10\%$ across several possible hadron parameterizations.

It is also worth noting that the present analysis utilized inclusive events in the MINOS detector. The inclusive charged-current cross section of ν_μ on iron is not well-known, so at present the analysis presented here cannot be turned into a flux measurement. However, if the same kind of analysis could be repeated using only a well-known scattering process like quasi-elastic scattering on lighter nuclei where reinteraction effects are less important, then the fitted event rate could be converted into a flux measurement. Such is the hope of the forthcoming MINERvA Run Plan.

References

- [1] Sacha E. Kopp, Žarko Pavlović, Patricia Vahle, “SKZP2: Update on Fitting the Beam MC to the ND Data,” March, 2006, updated in November, 2006, originally introduced in [3].
- [2] Sacha E. Kopp, Žarko Pavlović, Dharmaraj Indurthy, MINOS-doc-1283, “Systematic Uncertainties in the NuMI Beam Flux”.
- [3] Sacha E. Kopp, Žarko Pavlović, Patricia Vahle, MINOS-doc-1548, “Fitting the ND Data to the MC” (March, 2006).
- [4] L.A. Ahrens *et al.*, “Determination of the Neutrino Fluxes in the Brookhaven Wide Band Beams,” *Phys. Rev.* **D34**, 75 (1986).
- [5] R.C.Allen *et al.*, *Phys. Rev.* **D47**, 11 (1993).
- [6] P. Astier *et al.*, “Prediction of neutrino fluxes in the NOMAD experiment,” *Nucl. Instr. Meth.* **A515**, 800 (2003).
- [7] K. McFarland *et al.*, “Measurement of $\sin^2 \theta_W$ from Neutrino Nucleon Scattering at NuTeV,” 33rd Rencontres de Moriond: Electroweak Interactions and Unified Theories, Les Arcs, France, 14-21 Mar 1998, [arXiv:hep-ex/9806013](https://arxiv.org/abs/hep-ex/9806013).
- [8] G.P. Zeller *et al.*, “A Precise Determination of Electroweak Parameters in Neutrino Nucleon Scattering,” *Phys. Rev. Lett.* **88**, 091802 (2002).
- [9] M. Kostin, S. Kopp, M. Messier, D. Harris, J. Hylen, A. Para, Fermilab-TM-2353-AD (2002), “Proposal for Continuously-Variable Beam Energy”.
- [10] C. Alt *et al.*, “Inclusive Production of Charged Pions in $p+C$ Collisions at 158 GeV/ c Beam Momentum,” [arXiv:hep-ex/0606028](https://arxiv.org/abs/hep-ex/0606028), submitted to *Eur. Phys. J. C* (2006).
- [11] R. Ospanov, MINOS-doc-2740, “CC selection with k-nearest neighbor algorithm”

- [12] D. Petyt, MINOS-doc-2736, “Description of simple likelihood-based PID”
- [13] M. Kostin, S. Kopp, M. Messier, D. Harris, J. Hylen, A. Para, NuMI-B-783, “Proposal for Continuously-Variable Beam Energy”.
- [14] S. Kopp, M. Kostin, R. Zwaska, NuMI-B-768, “Hadron Production Models, Revisited”.
- [15] M. Messier *et al.*, NuMI-B-700, “Neutrino Fluxes and the Hadron Hose”.
- [16] J. Hylen *et al.*, ”Proposal to Include the Hadron Hose in the NuMI Beam”, NuMI-B-542.
- [17] N.V. Mokhov, “The MARS Monte Carlo”, Fermilab FN-628 (1995); O.E. Krivosheev *et al.*, Proc. of the Third and Fourth Workshops on Simulating Accelerator Radiation Environments (SARE3 and SARE4), Fermilab-Conf-98/043(1998) and Fermilab-Conf-98/379(1998).
- [18] M. Bonesini, A. Marchionni, F. Pietropaolo, and T. Tabarelli de Fatis, “On Particle Production for High Energy Neutrino Beams,” Eur. Phys. J. **C20**, 13-27 (2001).
- [19] *GEANT Detector Description and Simulation Tool*, CERN Program Library, W5013 (1994).
- [20] C.L. Wang, Phys. Rev. **D10**, 3876 (1974).
- [21] G. Cocconi *et al.*, LBL Report No. UCRL 10022 (1961).
- [22] A.J. Malensek, ”Empirical Formula for Thick Target Particle Production,” Fermilab-FN-341 (1981).
- [23] G. Collazuol, A. Ferrari, A. Guglielmi, P.R. Sala, Nucl. Instr. Meth. **449**, 609 (2000). A. Ferrari and P.R. Sala, ATLAS Internal Note ATLAS-PHYS-97-113, Proc. of the Workshop on Nuclear Reaction Data and Nuclear Reactors Physics, Design and Safety, ICTP, Trieste, Italy 1996. Publ. by World Scientific, A.Gandini, G.Reffo, eds.; P. Sala, talk given at the *2nd International Workshop on Neutrino Beams and Instrumentation*, 6-9 September, 2000, Batavia, IL.
- [24] All documentation and code from the Beam Systematics Group is available from the following web URL: <http://www.hep.utexas.edu/numi/beamMC>.
- [25] S. Kopp, L. Loiacono, minos-doc-2854, “Proton Beam Quality: Before and After the 2006 Accelerator Shutdown”
- [26] Numerical recipes in C

A *Ab Initio* Hadron Production Errors

To estimate the uncertainty of neutrino flux prediction before the fit to Near Detector data, we performed two studies which are described in this Appendix. First, we looked at different hadron production models and changes in near flux and far over near ratio (Section A.1). Different hadron production models predict different underlying pion p_T distributions. Second, we reweighted the target hadrons and changing the p_T distributions explicitly (Section A.2).

A.1 Model Spread

This section repeats some the studies performed previously in [14, 15, 16]. Here we study what the uncertainty on predicted flux if we just use the nominal beam Monte Carlo simulation, considering several models such as MARS[17], BMPT[18], Geant/Fluka[19], Malensek[22]. While looking at the spread of models does not give us the true uncertainty because some of the models are correlated and some have known flaws at certain kinematic region, it does gives us a feeling for this uncertainty. Other models, such as the Malensek[22], Sanford-Wang[20], and CKP[21], are probably not appropriate for comparison because the are phenomenological models tuned to different energies.

Figure 25 shows CC events in Near Detector using different hadron production models. Having in mind known flaws of certain models we estimate the error on the flux at Near Detector due to Hadron Production to be approximately 8% in the focusing peak and 15% in the tail. Figure 26 shows the effect of Hadron production uncertainty on Far over Near Ratio for three different beams (LE, pME and pHE). At high energies all 3 beams should approach same uncertainty since at high energies there is no horn focusing. Fluctuations are therefore, actually statistical fluctuations in Monte Carlo, so we apply some smoothing. We also disregard the gfluka at high energies since its known that it exaggerates the particle flux at high x_F .

It is also worth noting that the hadron production uncertainty, while over-estimated by virtue of our including some less credible models such as Geant/Fluka, is also potentially underestimated due to correlations between the models. In particular, the high energy tail, which has a strong contribution from kaon decays, could have an additional uncertainty because the kaon description in Fluka and MARS appears to be quite similar.

A.2 Particle Reweighting

Table 1 shows the mean transverse momentum of pions created in a graphite target by a proton beam of 120 GeV. The table compares the $\langle p_T \rangle$ from several models of hadron production, including some which are "disfavored" by current particle production data (though we have not specifically endeavored to understand the level of consistency or inconsistency). Because the NuMI horns focus particles most efficiently at $p_T \sim 250$ MeV/c, the spread in the models shown results in a varying yield of neutrinos if these various models are used

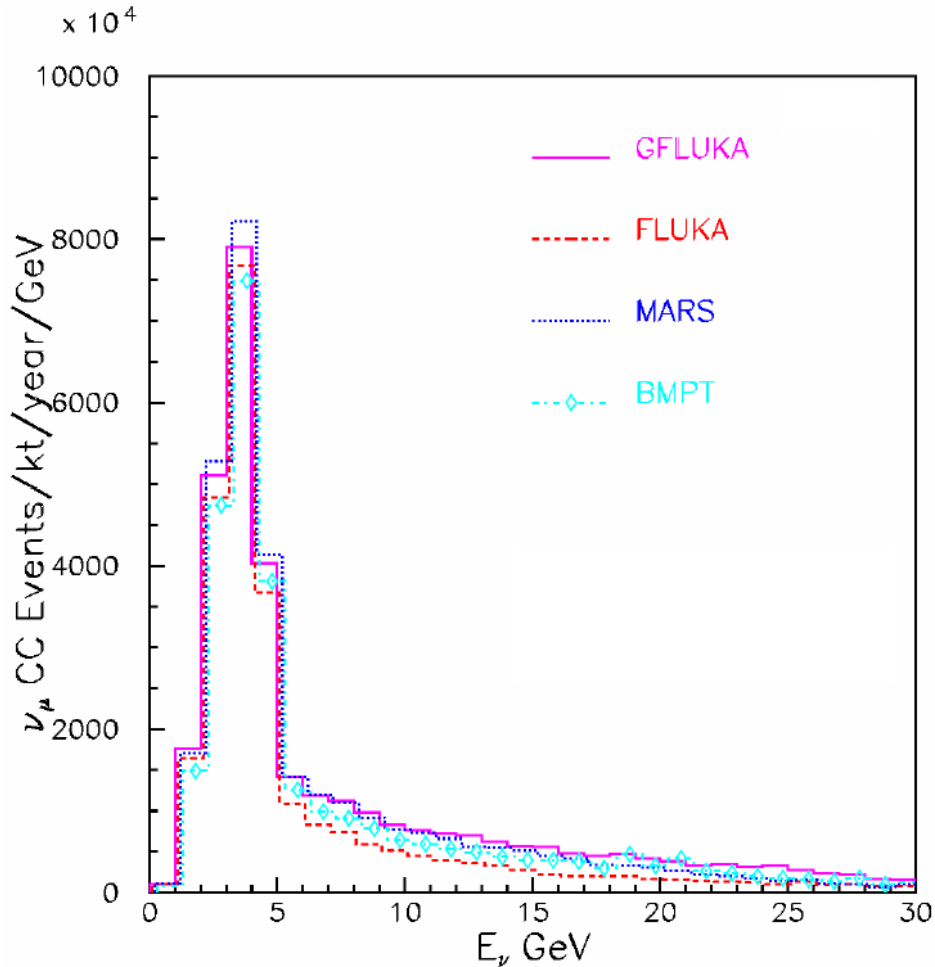


Figure 25: Hadron production model spread for LE beam at near detector.

as inputs to the beam MC: models predicting a narrow p_T spectrum would be expected to translate to a greater neutrino flux per proton on target.

We attempted to cross check our hadron production uncertainty by simply reweighting the target pions and kaons to give stiffer or softer p_T spectra. Figure 27 shows the pion transverse momentum distributions taken from the two Monte Carlos, MARS-v.15 and FLUKA-2005, used in GNuMI-v.18. As is indicated in the table, MARS predicts a softer p_T spectrum (which translates to a higher neutrino flux), with $\langle p_T \rangle = 380$ MeV/ c , as compared to FLUKA which has $\langle p_T \rangle = 430$ MeV/ c . We therefore skewed the FLUKA p_T distribution so as to give shifts in $\langle p_T \rangle$ comparable to the difference between MARS and FLUKA. As can be seen in the Figure, the skewed FLUKA distribution is similar to the MARS p_T distribution.

Figure 28 shows the transverse momenta of pions which result in neutrinos in the ND. That is, it is the same distribution as Figure 27, but with an extra neutrino weighting applied from the beam MC. As expected, the mean p_T is shifted downward, reflecting the selection

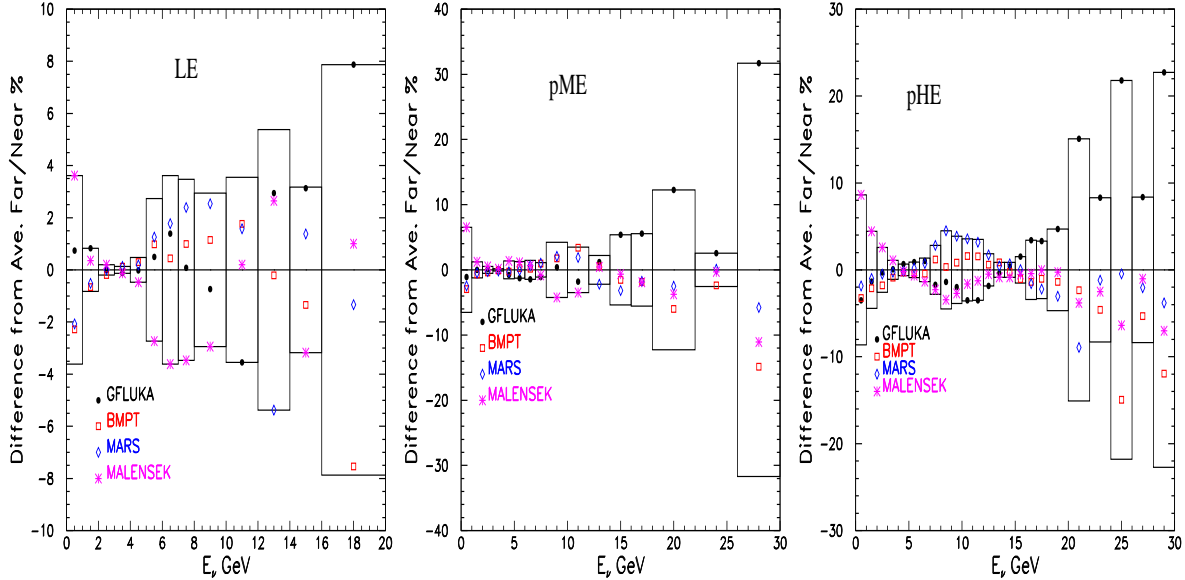


Figure 26: Hadron production model spread for Far over Near ratio.

by the focusing horns. We again show the spectrum distorted by ± 25 MeV and ± 50 MeV. Because the horn focusing reduces $\langle p_T \rangle$ by almost half, we will take the maximum allowable p_T shifts to be ± 25 MeV,

Figures 29 and 30 show what happens to the ND CC spectrum when $\langle p_T \rangle$ is shifted as in Figure 28. As can be seen, a shift of $\langle p_T \rangle$ by 25 MeV changes the neutrino flux in the focusing peak changes by $\sim 5 - 10\%$, while in the high energy tail it changes by 15-20%. This is consistent with the estimated flux error from hadron production estimated by the spread of various models. It is of interest to note that skewing the p_T distribution in the pME and particularly the pHE beams seems to have the effect of making a softer or harder neutrino spectrum. The sign of the effect is that a broadened p_T spectrum with $\langle p_T \rangle = 332$ MeV shows a softer neutrino spectrum. This is reasonable, since the pions with broadened p_T enter the decay volume with larger angles, so the decay angles of neutrinos hitting the ND must be larger, and this reduces the neutrino energy.

Figures 31 and 32 show the effect of this same p_T skewing on the F/N ratio. Similar to the systematic error derived from the spread of models, this skewing of the parent particles would seem to suggest that the F/N ratio is stable at the 5% level in the focusing peak for the worst-case of the pHE beam, and is better than 3% in the LE beam. The spread F/N in the high energy tail is a about 5%.

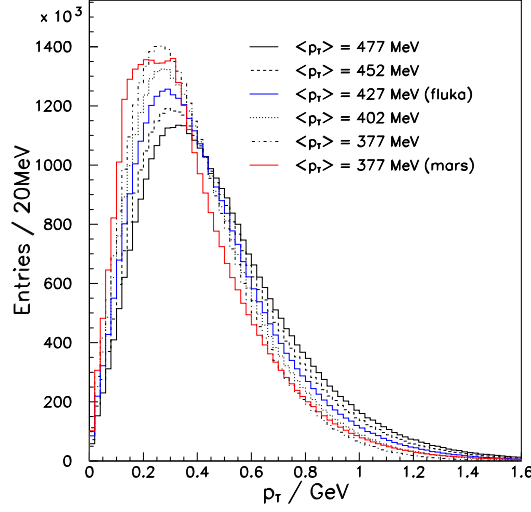


Figure 27: Transverse momentum of pions created in a graphite target by a proton beam of 120 GeV, as predicted by the FLUKA-2005 and MARS-v.15 Monte Carlos. Also shown are several versions of the FLUKA distribution skewed to shift $\langle p_T \rangle$.

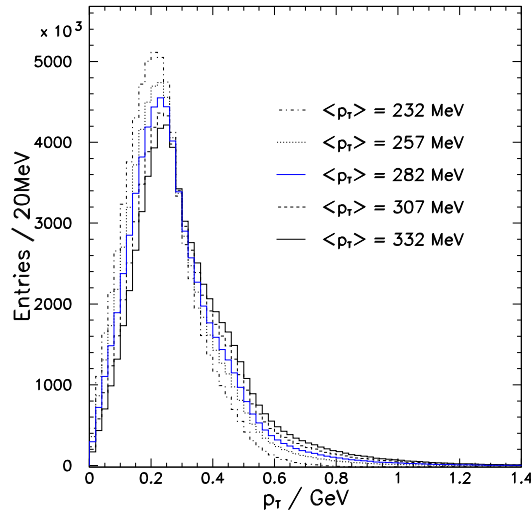


Figure 28: Transverse momenta of particles from the target as predicted by FLUKA-2005, but for only those particles which produce a CC neutrino interaction in the ND (*cf.* Figure 27).

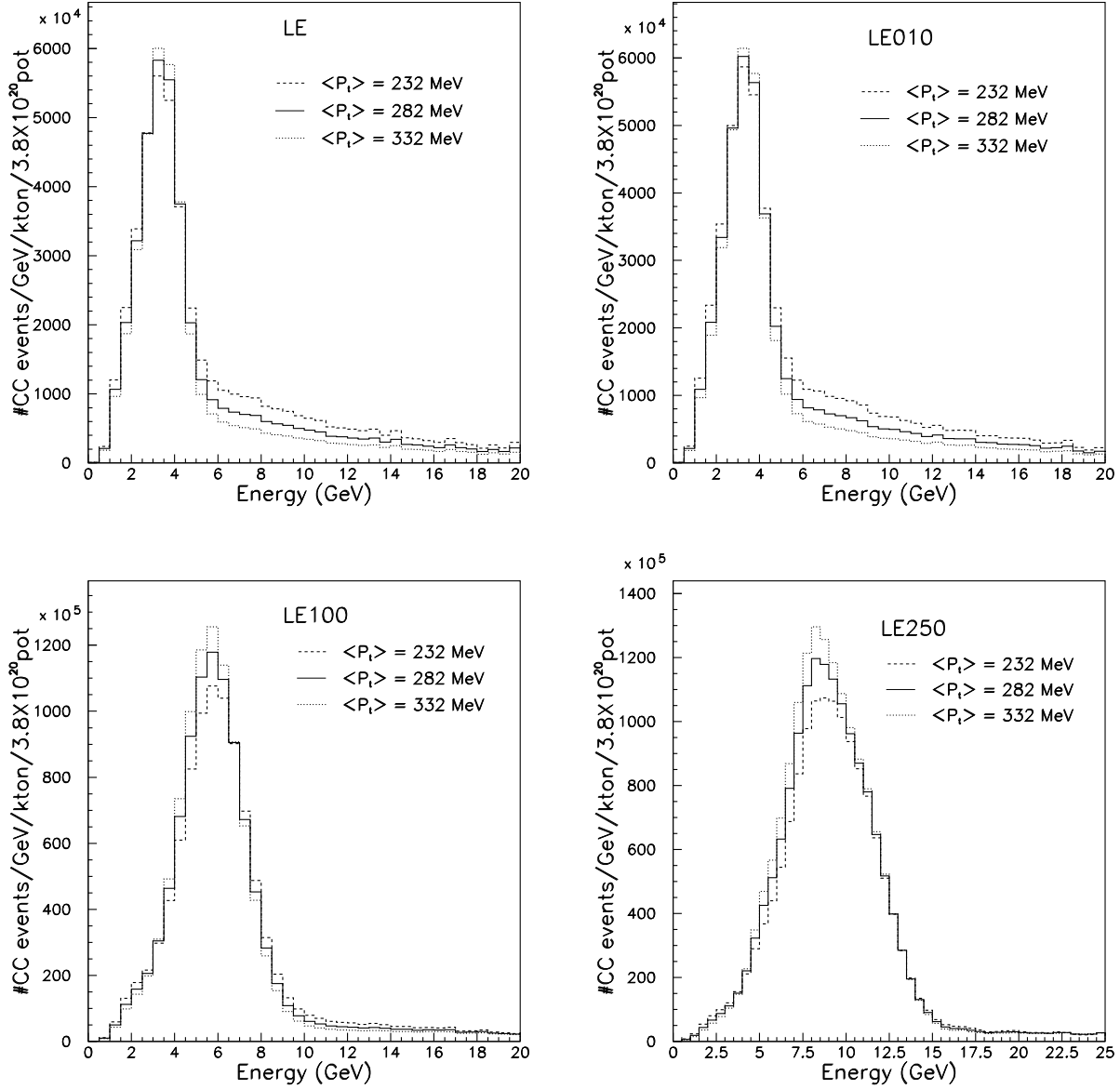


Figure 29: Neutrino spectra in the ND as predicted from GNuMI-v.18 (FLUKA-2005) in the LE (top left), LE10 (top right), pME (bottom left), and pHE (bottom right). In each plot, the nominal pion $\langle p_T \rangle$ of 282 MeV/ c has been skewed by ± 50 MeV/ c .

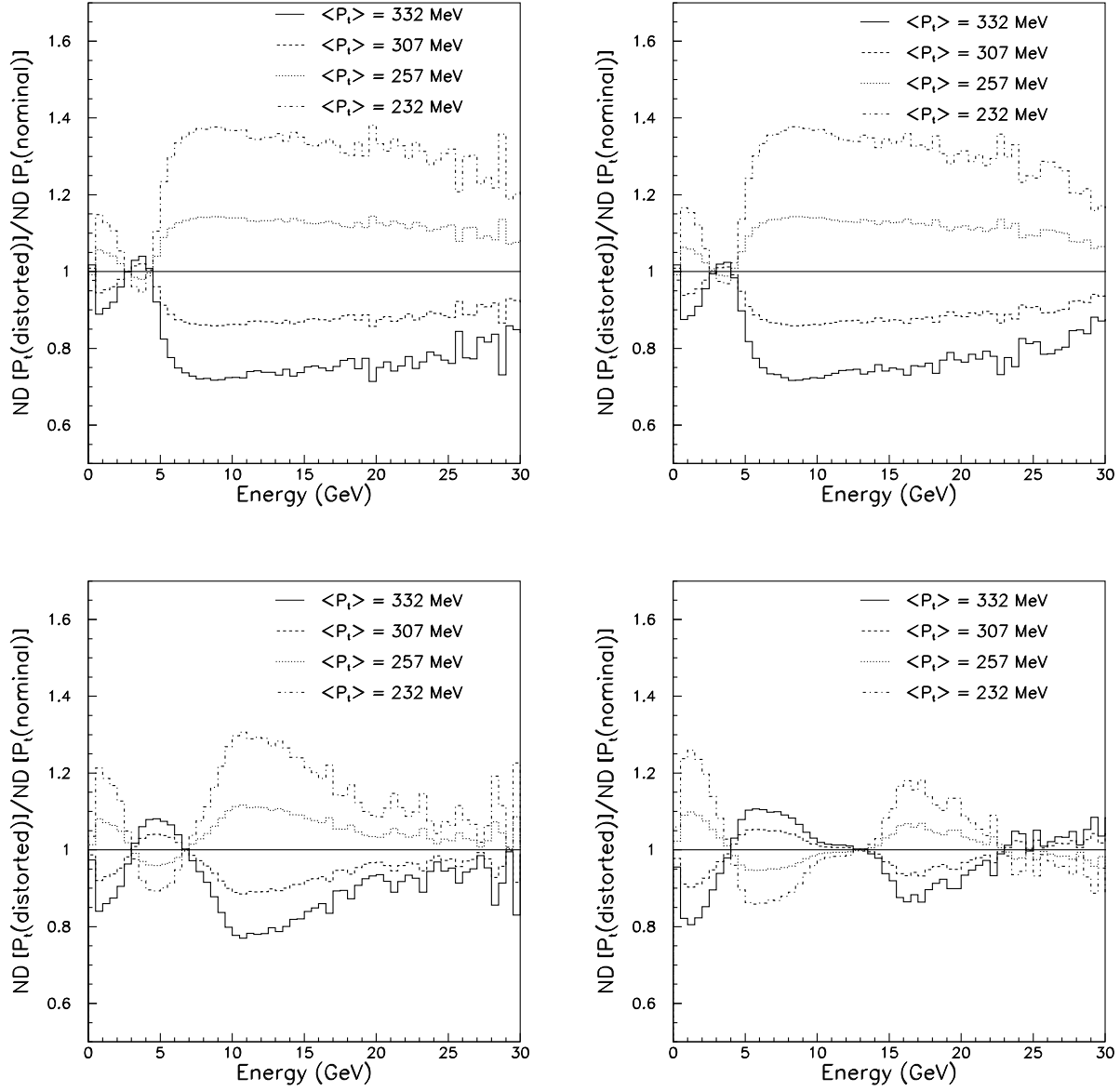


Figure 30: Ratio of neutrino spectra in the ND as predicted from the skewed p_T spectra of Figure 29 to the nominal spectra generated with $\langle p_T \rangle = 282 \text{ MeV}/c$.

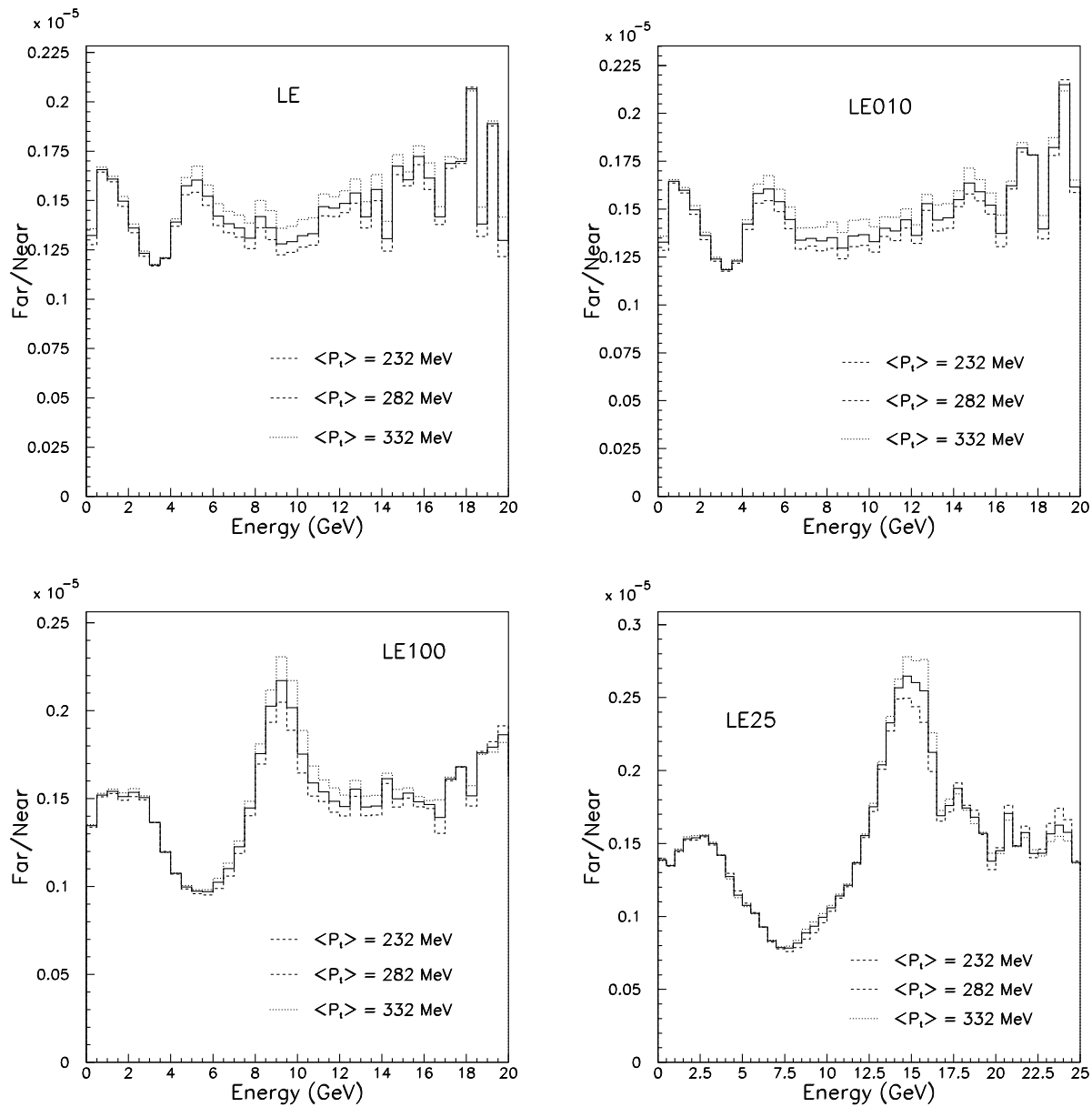


Figure 31: F/N ratio as predicted from GNuMI-v.18 (FLUKA-2005) in the LE (top left), LE10 (top right), pME (bottom left), and pHE (bottom right). In each plot, the nominal pion $\langle p_T \rangle$ of 282 MeV/c has been skewed by ± 50 MeV/c.

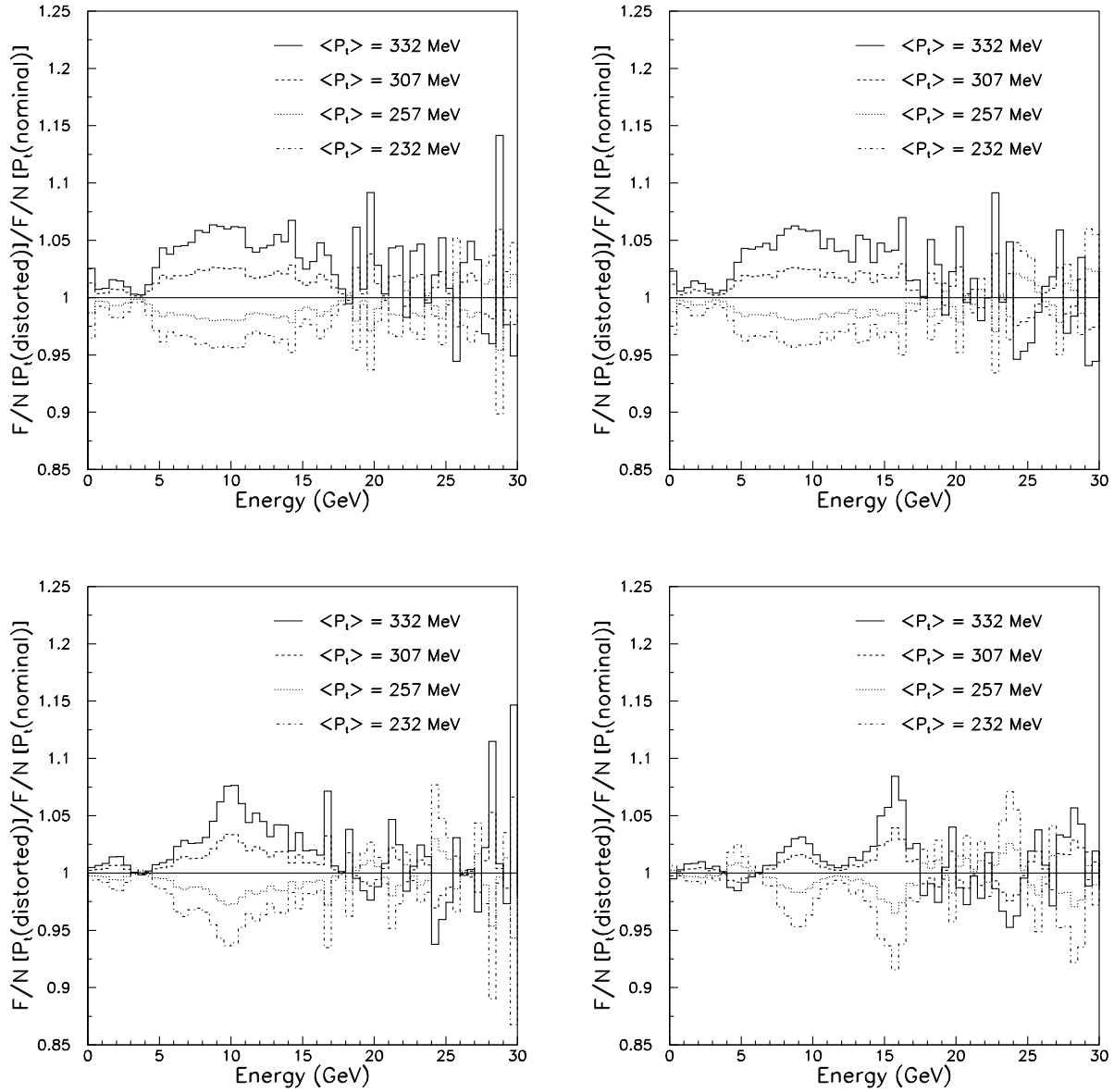


Figure 32: Double-ratio of F/N ratio as predicted from the skewed p_T spectra of Figure 31 to the nominal spectra generated with $\langle p_T \rangle = 282$ MeV/ c .